Journal of Inflammation Research

Dovepress
Taylor & Francis Group

Open Access Full Text Article

ORIGINAL RESEARCH

Characterization of Cuproptosis-Related LncRNAs Prognostic Signature and Identification of LINC02285 as a Novel Biomarker for Ovarian Cancer

Han Lei[1], Zhengwei Zhou[1], Chang Liu[2], Weiting Chen[2], Yu Li[3], Guang Shu[1], Maonan Wang[1], Ke Guo[4], Qiong Pan[5], Gang Yin[1,6,7]

[1]Department of Pathology, Xiangya Hospital, Xiangya School of Basic Medical Science, Central South University, Changsha, People's Republic of China; [2]Xiangya School of Basic Medical Science, Central South University, Changsha, People's Republic of China; [3]Intensive Care Unit for Children, Xiangtan Central Hospital, Xiangtan, People's Republic of China; [4]Department of Neurology, The Third Xiangya Hospital of Central South University, Changsha, People's Republic of China; [5]Department of Obstetrics and Gynecology, The Third Xiangya Hospital of Central South University, Changsha, People's Republic of China; [6]China-Africa Research Center of Infectious Diseases, Xiangya School of Basic Medical Science, Central South University, Changsha, People's Republic of China; [7]National Clinical Research Center for Geriatric Disorders, Xiangya Hospital, Central South University, Changsha, People's Republic of China

Correspondence: Qiong Pan; Gang Yin, Email 1517682924@qq.com; gangyin@csu.edu.cn

Background: Cuproptosis, a novel form of cell death triggered by copper ion accumulation, has shown potential in cancer therapy, particularly through the involvement of cuproptosis-related lnRNAs (CRLs). In-depth analyses exploring the relationship between CRLs and ovarian cancer (OC) are currently limited.

Methods: LASSO-Cox regression analysis was conducted to assess the prognostic significance of CRLs and develop a cuproptosis-related prognostic model. Furthermore, tumor immune microenvironment and drug sensitivity were analyzed using ssGSEA, GSVA, ESTIMATE, and CIBERSORT algorithms. Finally, the tumorigenic effect of LINC02285 in OC and its correlation with cuproptosis were investigated by in vitro cell experiments.

Results: We identified 138 CRLs correlated with cuproptosis-related genes (CRGs), 4 key CRLs (AC080038.1, AC083880.1, LINC00861, and LINC02285) were used to develop a prognostic model that effectively distinguished between low-risk and high-risk patients with significant differences in overall survival and progression-free survival. ROC curve analysis further validated the predictive capacity of the signature. Additionally, the low-risk group had a favorable prognosis associated with a protective immune microenvironment and a better response to targeted drugs. Conversely, the high-risk group displayed aggressive tumor features and poor immunotherapy outcomes. Validation through qPCR confirmed the differential expression of these CRLs in OC cells compared to normal ovarian cells, underscoring their potential significance in tumor biology. Bioinformatics analyses corroborated the association of LINC02285 with poor prognosis in OC patients. Functional experiment results showed that abnormal expression of LINC02285 could significantly regulate the proliferation and migration of OC cells. In addition, overexpression of LINC02285 markedly attenuated the inhibitory effects of Elesclomol-$CuCl_2$ on OC cell activity.

Conclusion: Our study established a prognostic model based on 4 CRLs to assess overall survival and the immune microenvironment in OC patients. As a high-risk factor, LINC02285 demonstrates potential as a prognostic biomarker for OC.

Keywords: ovarian cancer, cuproptosis, linc02285, prognostic signature, tumor microenvironment

Introduction

Ovarian cancer (OC) is one of the most common malignancies of the reproductive system, ranking second in mortality after cervical cancer, and seriously affecting the health of women worldwide.[1] About 60–70% of patients with OC are already in stage III–IV at diagnosis, treatment is difficult, the prognosis is poor, and the 5-year overall survival rate is

Received: 8 February 2025
Accepted: 27 May 2025
Published: 8 June 2025

about 40%.[2] The high mortality rate of OC is largely due to the lack of effective biomarkers for early detection and prognosis. Although CA125 and HE4 are currently the most commonly used biomarkers for OC, their sensitivity and specificity are low, they cannot effectively distinguish between benign and malignant tumors, and their effectiveness in the detection early.[3–5] Hence, it is imminent to find promising biomarkers for predicting OC prognosis and develop effective therapeutic strategies.

Copper is an essential trace element involved in numerous biological processes, but both deficiency and excess copper can cause significant damage to cellular function. Some studies have shown that decreased serum copper levels are associated with the development of endometrial cancer,[6] and disruptions in copper homeostasis have also been observed in the progression of head and neck cancers.[7] Recently, a novel cell death pathway known as cuproptosis has gained attention. Research has demonstrated that copper directly binds to the lipoylated components of the tricarboxylic acid (TCA) cycle, inducing toxic protein stress and ultimately leading to cell death.[8] Given copper's dual role as both an essential enzyme co-factor and a potential source of toxicity, it is emerging as a promising therapeutic target to selectively kill cancer cells by promoting intracellular copper accumulation.[9–11] This offers significant implications for the development of new cancer therapies based on this regulatory pathway.

Since the concept of cuproptosis was proposed, many researchers and research institutions have devoted themselves to exploring its application in cancer treatment, and remarkable progress has been made, especially in the field of long non-coding RNAs (lncRNAs) associated with cuproptosis.[12,13] In recent decades, accumulating evidence has highlighted the critical role of lncRNAs as regulatory molecules in tumorigenesis.[14–17] However, the functions of many lncRNAs in OC remain poorly understood. Although there have been reports suggesting a link between cuproptosis-related lnRNAs (CRLs) and OC,[18,19] conclusive evidence supporting this association is still lacking. Most of the current studies on CRLs in the field of OC focus on building prognostic models based on CRLs expression levels, rather than confirming the relationship between specific lncRNAs and copper death at the cellular level.[20,21] Thus, our study focuses on CRLs, seeking to understand their role in OC and identify potential therapeutic targets for OC.

In this study, we aimed to develop the CRLs signature to independently refine OC prognosis prediction and to identify high-risk patient subgroups most likely to benefit from adjuvant therapies. We systematically characterized CRLs, developed a risk model for predicting OC prognosis using the TCGA datasets, and identified 4 differentially expressed CRLs. Functional enrichment and immune infiltration analyses were carried out to determine the potential molecular mechanism, and its potential value in evaluating prognosis, diagnosis, tumor immune infiltration, immunotherapy response, and chemotherapy efficacy was explored, followed by internal validation and external verification. Moreover, to further understand the mechanism of CRLs in OC, we selected the risk factor LINC02285 (hazard ratio=2.404) as a representative candidate factor to reveal its effects on OC cell proliferation and migration by cell function assays. Subsequently, cell viability assays also confirmed LINC02285's regulatory impact on cuproptosis sensitivity.

Our findings provide new insights into the biological functions and molecular mechanisms underlying cuproptosis in OC, while also highlighting the potential therapeutic benefits of immunotherapy for OC patients. Furthermore, through a series of in vitro cellular experiments, we demonstrate that key CRLs, particularly LINC02285, significantly influence OC cell proliferation, migration, and sensitivity to cuproptosis.

Materials and Methods

Multiomics Data Source and Preprocessing

Figure 1 presents a flowchart of our research methodology. We obtained clinical information data and somatic mutation data of OC patients from The Cancer Genome Atlas (TCGA) database (https://portal.gdc.cancer.gov/). Oncoplot was drawn according to the descending order of mutations using the R package "maftools".[22] The copy number variation (CNV) data and RNA-Seq data of normal ovarian samples and OC patients were obtained from the UCSC Xena server[23] (http://xena.ucsc.edu/). A total of 379 OC patients and 88 normal ovarian samples were involved in the present study. Then, Ensembl IDs were converted to official gene symbols, and log2 processing of the data was performed. LncRNAs and protein-coding genes were screened by the Ensembl human genome browser GRCh38. The clinical characteristics of

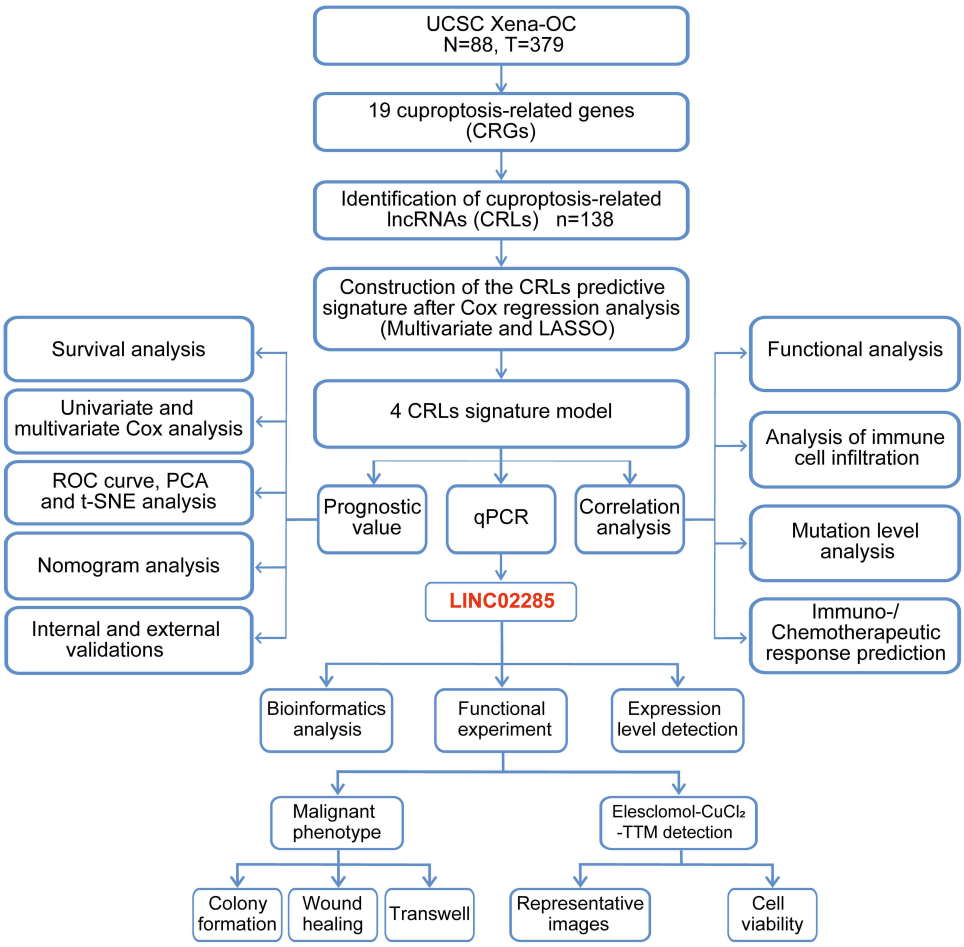

Figure 1 Flowchart of the Study.

the patients are shown in Table S1. Study participants with incomplete clinical information were excluded. OC data for Ovarian cancer-Australia OV-AU items were collected from the International Cancer Genome Consortium (ICGC, https://icgc.org) database. A total of 85 samples were included in the column as an independent external verification cohort for analysis.

Construction of Cuproptosis-Related Prognosis Model in OC

Cuproptosis-related genes (CRGs) were obtained from a literature search.[8,9,24,25] To identify CRLs, we used the "limma" package to calculate the correlation between CRGs and lncRNAs. Using the correlation coefficient $|R_2|>0.4$ and $p<0.001$ as the screening criteria, a total of 138 CRLs with expression values were obtained. We first used univariate Cox regression analysis to obtain CRLs related to the prognosis of OC patients, and then we carried out multivariate Cox regression analysis and least absolute shrinkage and selection operator (LASSO) Cox regression to construct the CRLs predictive signature. Finally, a risk score for each individual was computed using this prognostic signature. The risk score was calculated using the following formula: risk score=(Coefficient lncRNA1 × expression of lncRNA1) + (Coefficient lncRNA2 × expression of lncRNA2) + ⋯ + (Coefficient lncRNAn × expression lncRNAn). Based on the median value of the risk score, the training cohort, the testing cohort, and all patients were classified into high-risk and low-risk groups, respectively.

Verification of Cuproptosis-Related Prognosis Model in OC

The Kaplan-Meier (KM) curve was used to compare the OS probability difference between high-risk groups and low-risk groups in the training cohort, testing cohort, and all patients respectively using the Log rank test with "survival" and

https://doi.org/10.2147/JIR.S521410

"survminer" packages. Receiver operating characteristic (ROC) was used to evaluate the accuracy of our model using the "survival", "survminer", and "timeROC" packages. The univariate and multivariate Cox regression analyses were used to determine the independent prognosis factors using the "survival" packages. Principal component analysis (PCA) and t-distributed stochastic neighbor embedding (t-SNE) analysis were used to visualize the data in two dimensions with the "Rtsne" and "ggplot2" packages. We combined the risk score with the clinicopathological characteristics of age and grade to construct a nomogram that can predict the 1-, 3- and 5-year survival of OC patients. A calibration curve to test whether the predicted survival rate was consistent with the actual survival rate.

Assessment of Immune Cell Infiltration and Immune Microenvironment

CIBERSORT is an analysis tool using expression data to represent the cell composition of complex tissues based on preprocessed gene expression profiles.[26] We calculated the ratio of each tumor-infiltrating immune cell in all patients using the CIBERSORT algorithm. The ESTIMATE algorithm was used to assess immune infiltration in OC patients. Single sample gene set enrichment analysis (ssGSEA) was used to evaluate the infiltration levels of immune cell types and immune function between the high-risk and low-risk groups in the R packages of "gsva". To evaluate the difference in tumor immune microenvironment between the high-risk group and low-risk group, immune functions, and each immune cell were compared between the high and low-risk groups. Tumor mutation burden (TMB)[27] and tumor immune dysfunction and exclusion (TIDE)[28] were also analyzed in the patients to predict their reactions to immunotherapy.

Mutation Status Analysis

We extracted the sample mutation data in the TCGA cohort. Then the R package "maftools" was used to analyze the mutation status between two risk groups.

Immuno-/Chemotherapeutic Response Prediction

Downloaded the OC immunotherapy score file from The Cancer Immunome Atlas (TCIA, https://tcia.at/) database to predict the clinical response to immune checkpoint inhibitors between the high-risk and low-risk groups. The "pRRophetic"[29] R package was used to predict the half-maximal inhibitory concentration (IC50) of chemotherapy drugs, this value indicates the effectiveness of a substance in inhibiting specific biological or biochemical processes. To evaluate the role of the predictive signature in predicting the response to OC treatment, we calculated the IC50 of common chemotherapy drugs applied for the clinical treatment of OC. The Wilcoxon signed-rank test was used to compare the IC50 values between the high-risk and low-risk groups.

Cell Culture and Transfection

All cell lines used in this study including the normal ovarian epithelial cells (IOSE), and OC cells (OV90, A2780, and SKOV3), were purchased from the American Type Culture Collection (ATCC, USA). These cells were cultured in RPMI-1640 (BI) replenished with 10% fetal bovine serum (FBS, BI), 100 μg/mL penicillin (Sigma), and 100 μg/mL streptomycin (Sigma). All cells were cultured at 37 °C in a humidified 5% CO_2 incubator. Cells were collected for the experiment at the indicated time. 5×10^5 OC cells were seeded in a six-well plate and then reached 60–70% fusion degree per well, jetPRIME was applied for transient transfection plasmid and/or siRNA in vitro according to manufacturer's instructions. These cells were digested and collected after 48 h of transfection for the subsequent assays. All of the sequences of primers are listed in Table S2.

RNA Isolation and qPCR

Total RNA was isolated using Trizol reagent (Vazyme, Nanjing, China). Complementary DNA (cDNA) was synthesized using the TransScript Uni All-in-One First-Strand cDNA Synthesis SuperMix for qPCR (One-Step gDNA Removal) (TransGen Biotech, AU341-02-V2). qPCR was performed by the Applied Biosystems 7500 Real-Time PCR System and the ChamQ Universal SYBR qPCR Master Mix (Vazyme, Q711-02). GAPDH was used as an endogenous reference. The sequences of primers used for qPCR are listed in Table S2.

Colony Formation Assay

OC cells were transfected with LINC02285 siRNA and LINC02285-OE for 36 h. 500 cells were seeded in a six-well plate and allowed to grow until visible colonies. After 10–14 days, cell colonies were washed with PBS, fixed with 4% paraformaldehyde for 30 min, and stained with crystal violet for 20 min. Image J was used to count the number of colonies per well.

Transwell Assay

Cell migration was measured by Transwell assays using the 24-well transwell chambers with 8 μm polycarbonate membranes (Corning Incorporated, USA). A total of 2×10^5 cells in 200 μL serum-free medium were added to the upper chamber. The lower chamber contained 800 μL medium with 20% FBS as a chemoattractant. After incubation for 24 h, the cells on the lower surface were fixed with 4% paraformaldehyde for 30 min and stained with crystal violet for 20 min. The relative cell number was calculated a light microscope (Olympus, Tokyo, Japan).

Wound Healing Assay

After being transfected with LINC02285 siRNA and LINC02285-OE for 24 h, OC cells were seeded into a 12-well plate and then scraped with a 200 μL pipette tip. Cell migration images were captured at 0, 24, 36, 48, 60, and 72 h after scratching.

Cell Viability Assay

Cells were inoculated into 96-well plates at a rate of 3000 cells/well and allowed to attach for 12 h. Elesclomol and copper chloride ($CuCl_2$) solution were added 1: 1 for 24 h. Then 100 μL of fresh medium containing 10% CCK8 solution was added and the 450nm absorbance was detected following incubation for 2 h at 37 °C using an enzyme-labeled apparatus. As for the chemical rescue assay, copper ion chelator (TTM) was added after plating overnight, then Elesclomol-$CuCl_2$ was added into plates and incubated for 24 h.

Statistical Analysis

We performed all statistical analyses using the R software (version 4.2.0) and GraphPad Prism software (version 9.0). Chi-squared test was performed for categorical data. Student's *t*-test and Wilcoxon rank-sum test were used to analyze the statistical significance between two groups, which test whether one of the two independent samples is significantly larger or smaller. Among them, the Student's *t*-test is suitable for normally distributed data, while the Wilcoxon rank-sum test is suitable for non-normally distributed variables. Pearson's correlation coefficient was utilized for correlation assessments. KM curve and Log rank test were adopted to assess whether there were differences in OS between groups. Statistical significance is indicated with asterisks (*). A two-sided p value of <0.05 was considered statistically significant (*p<0.05, **p<0.01, ***p<0.001, ****p<0.0001).

Results

Molecular Characterization of CRGs in OC Patients

To investigate the correlation between cuproptosis-related lncRNAs (CRLs) and OC, we compiled a list of 19 cuproptosis-related genes (CRGs)—NFE2L2, NLRP3, ATP7B, ATP7A, SLC31A1, FDX1, LIAS, LIPT1, LIPT2, DLD, DLAT, PDHA1, PDHB, MTF1, GLS, CDKN2A, DBT, GCSH, and DLST—from published articles.[8,9,24,25] The expression levels of these 19 CRGs in normal and tumor tissues are shown in Figure 2A, based on data from 88 normal and 379 tumor samples in the GTEx and TCGA databases. A correlation network depicting the relationships between the CRGs is presented in Figure 2B, with red indicating positive correlations and blue indicating negative correlations. An overview of the mutation changes in CRGs in OC patients revealed that 25 of 462 (5.63%) OC patients exhibited cuproptosis-associated genetic mutations (Figure 2C). Among these, NLRP3 (2%) and ATP7B (1%) had higher mutation frequencies compared to the other genes (Figure 2C). The CNV frequencies of CRGs in OC patients are shown in Figure 2D, while the locations of altered CNVs on the respective chromosomes of these genes are illustrated in Figure 2E.

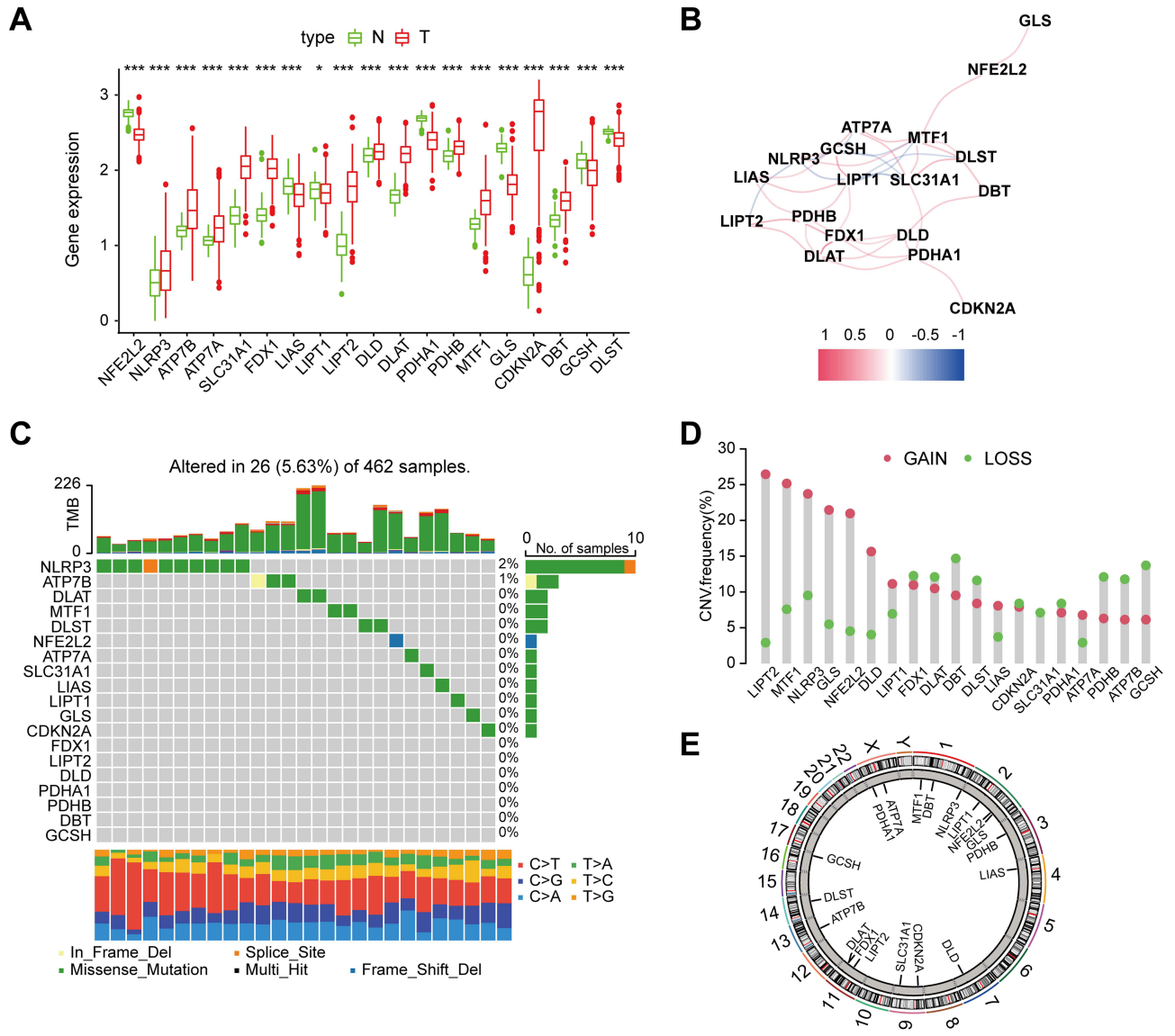

Figure 2 Molecular Characterization of CRGs in OC Patients. (**A**) The expression of 19 CRGs in OC tissues and normal tissues (tumor in red and normal in green). The upper and lower ends of the boxes represent the interquartile range of values. The lines in the boxes represent the median value. (**B**) The correlation network of the CRGs (red line: positive correlation; blue line: negative correlation. The depth of the color reflects the strength of the relevance. (**C**) In each waterfall plot, mutation information is presented for each gene associated with cuproptosis, and each mutation type is indicated by the color at the bottom. In the above-mentioned bar chart, the numbers on the left represent the mutation burden whereas on the right are the mutation frequencies. (**D**) The CNV frequency of CRGs in OC patients from the TCGA cohort. The height of each column represented the alteration frequency. The amplification frequency, pink dot; The deletion frequency, blue dot. (**E**) Position of altered CNV of CRGs in CRGs on 23 chromosomes. *p<0.05, **p<0.01, ***p<0.001.

Construction of the CRLs Prognostic Signature in OC

After reviewing the literature, we identified 19 CRGs, which were then used to calculate 138 CRLs (Figure 3A). Detailed information is provided in Table S3. The expression levels of these 138 CRLs in OC and normal tissues are presented in Figure 3B, with tumor samples shown in red and normal tissues in green. Univariate Cox regression analysis identified 4 CRLs (AC080038.1, AC083880.1, LINC00861, and LINC02285) significantly associated with the prognosis of OC patients (Figure 3C). To minimize overfitting during signature generation, we performed LASSO-Cox regression analysis, which ultimately confirmed these 4 CRLs as the key components of the prognostic signature (Figure 3D and E).

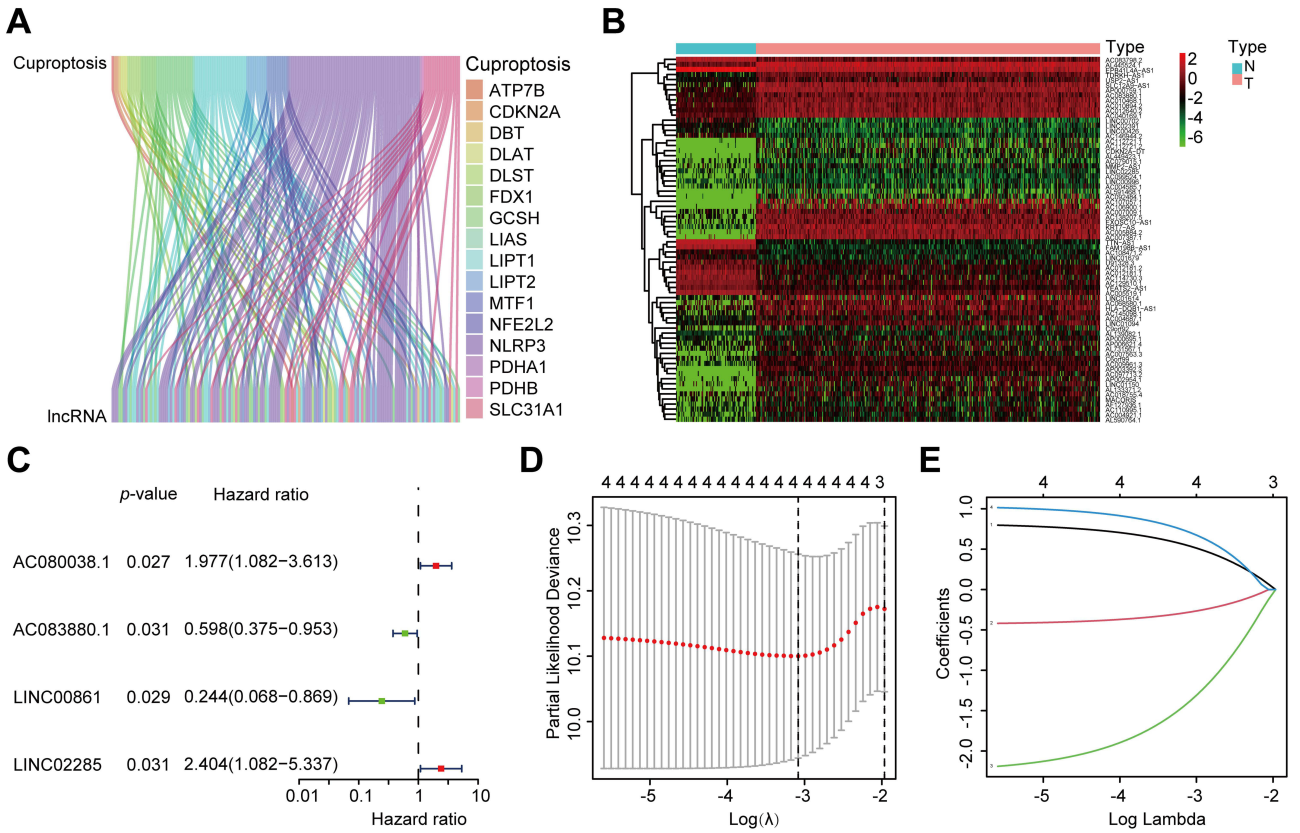

Figure 3 Construction of the CRLs Prognostic Signature in OC. (**A**) 138 CRLs correlated with 19 CRGs. (**B**) The expression of 138 CRLs in OC and normal tissues (tumor in red and normal in green). (**C**) The univariate Cox regression analysis between CRLs and OS of OCs is shown in the forest plots. The *P*-values were obtained by univariate Cox regression. (**D**) According to the minimum criteria, 4 CRLs were selected by the LASSO regression model. (**E**) In LASSO regression, the coefficients of CRLs were calculated.

Construction and Validation of the CRLs Signature Model in the Training, Testing, and All Cohort

To evaluate the prognostic value of these CRLs, samples from the TCGA-OC database were randomly divided into two cohorts: a training cohort and a validation cohort. The clinical characteristics of the samples in both cohorts are summarized in Table S4. The results showed no significant bias in tumor grade (p=0.5724) or age (p=0.3717) between the two cohorts, indicating that the study was conducted with random and rational grouping. In this model, each OC patient in the TCGA database was assigned a risk score using the following formula: Risk Score=AC080038.1*0.821351 + AC083880.1*(−0.431257) + LINC00861*(−2.267466) + LINC02285*1.039265 (Note: the name of lncRNA indicates their expression level in TCGA database).

We next assessed the prognostic value of the 4 CRLs model. The samples in the training cohort were classified into high-risk (n=93) and low-risk (n=93) groups based on the median risk score. Figure 4A displays the expression profiles of candidate lncRNAs across patients in the training cohort, whereas Figure 4D illustrates the risk score distribution between high- and low-risk groups. As risk scores increased, mortality rates also rose (Figure 4G). A time-dependent ROC curve was generated for the training cohort, yielding areas under the curve (AUC) of 0.616 at 1 year, 0.631 at 3 years, and 0.657 at 5 years (Figure 4J). KM analysis further revealed that OS was significantly poorer in the high-risk group compared to the low-risk group (Figure 4M). To further assess the accuracy of the CRLs signature, we calculated a risk score for each individual in the testing cohort using the same formula applied in the training cohort. Patients were then classified into high-risk (n=84) and low-risk (n=102) groups based on the same cut-off values used in the training cohort. The distributions of the 4 CRLs and risk scores were similar in both the heatmap and the risk score distribution (Figure 4B–E). Higher risk scores were

https://doi.org/10.2147/JIR.S521410

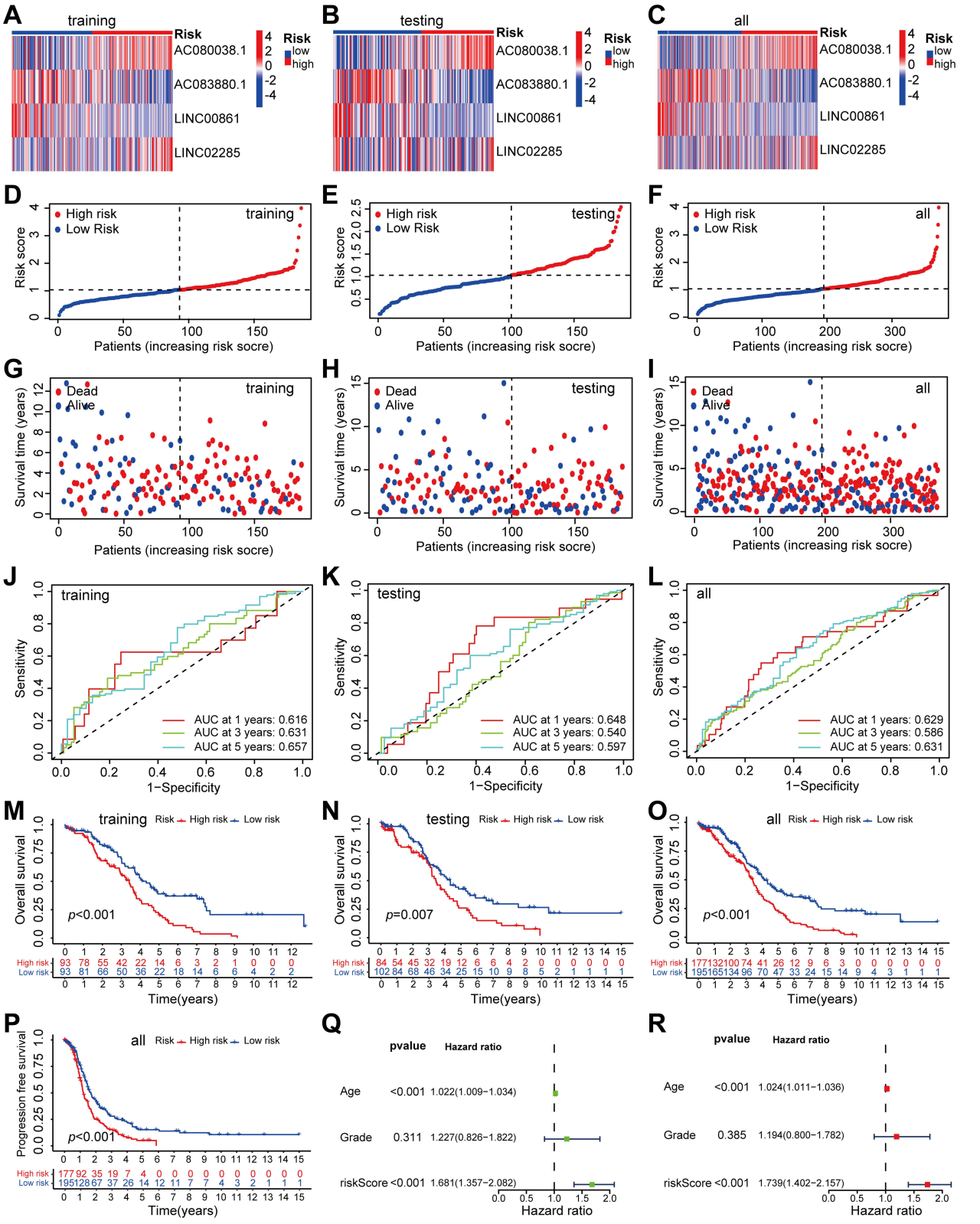

Figure 4 Construction and Validation of the CRLs Signature Model in the Training, Testing, and All Cohort. (**A**–**C**) The expression heatmap of 4 CRLs in the training cohort, testing cohort, and all patients. (**D**–**F**) The distribution of the risk scores in the training cohort, testing cohort, and all patients. (**G**–**I**) In the training cohort, testing cohort, and all patients, the scatter plots show whether the samples were alive or not. Blue represents the number of survivors, and red represents the number of deaths. (**J**–**L**) The prognostic accuracy of the risk scores in the training cohort, testing cohort, and all patients were verified by the ROC curve. ROC, receiver operating characteristic. (**M**–**O**) The KM curves depict the OS in high-/low-risk groups in the training cohort, testing cohort, and all patients. (**P**) The KM curves depict the PFS in high-/low-risk groups in all patients. (**Q**–**R**) Univariate (**Q**) and Multivariate (**R**) Cox regression analysis of clinical features and risk score in OC samples.

associated with fewer survivors and a greater number of deaths (Figure 4H). The AUC values for the 4 CRLs signature in predicting 1-, 3-, and 5-year survival rates were 0.648, 0.540, and 0.597, respectively (Figure 4K). KM analysis confirmed that high-risk CRLs signatures were significantly associated with poorer survival outcomes (Figure 4N).

Similar to the results obtained from the training and testing cohort, consistent findings were observed when comparing all patients using the same cut-off values. Figure 4C, F and I present the expression profiles of the 4 CRLs signatures, the distribution of risk scores, and the survival status of patients. ROC curve analysis of the TCGA-OC cohort demonstrated that our model exhibited strong predictive performance, with AUC values of 0.629 for 1 year, 0.586 for 2 years, and 0.632 for 3 years survival (Figure 4L). KM analysis revealed that patients in the high-risk group had significantly shorter survival compared to those in the low-risk group (Figure 4O). In addition, unlike most prognostic models that primarily focus on OS, our study also included progression-free survival (PFS), which may reflect reductions in tumor burden and symptom relief.[30,31] KM analysis further confirmed that PFS was markedly worse in the high-risk group compared to the low-risk group (Figure 4P).

To assess whether the predictive signature is an independent prognostic factor for OC patients, we conducted a Cox regression analysis. Univariate Cox regression revealed that the risk score of this signature was significantly associated with OS rates in OC patients (Figure 4Q). Multivariate Cox regression further identified that the 4 CRLs risk signatures, along with age, could independently predict OS rates in OC patients from the TCGA database (Figure 4R).

Distribution Heatmap and KM Survival Curves of Clinicopathological Variables in the High-/Low-Risk Groups

To enhance the clinical applicability of the predictive model, we integrated clinical data and gene expression features from TCGA-OC. We analyzed the association between the CRLs' prognostic signature and clinicopathological characteristics. The gene expression profiles and clinical features, including tumor differentiation (G1-G4) and age (≤65 or>65 years), are presented in a heatmap. However, we observed minimal differences in clinical features between the high-risk and low-risk groups (Figure S1A). The distribution of clinicopathological variables in the high-/low-risk groups is shown in Figure S1B and C. To investigate the relationship between the predictive signature and the prognosis of OC patients based on various clinicopathological factors, patients were stratified by grade (Figure S1D) and age (Figure S1E). In all classifications, patients in the high-risk group had significantly shorter OS compared to those in the low-risk group. These findings suggest that the predictive signature can effectively assess the prognosis of OC patients, independent of clinicopathological variables.

Prognostic Analysis of the 4 CRLs Risk Model in TCGA and ICGC Cohorts

The prognostic risk score, along with age and tumor grade, was used to generate a ROC survival curve. The results showed that the CRLs-based prognostic risk scoring system accurately predicted the 1-, 3-, and 5-year survival rates of OC samples, outperforming other clinical traits (Figure 5A; AUC=0.629, 0.586, and 0.631, respectively). To further refine prognosis prediction, we developed a nomogram incorporating clinicopathological variables and the risk score. This nomogram successfully predicted the 1-, 3-, and 5-year survival outcomes for OC patients (Figure 5B). The calibration curves demonstrated good consistency between the observed OS rates and the predicted survival rates at 1, 3, and 5 years (Figure 5C). PCA and t-SNE analysis further confirmed distinct distributions of patients in the high-/low-risk groups (Figure 5D and E). Additionally, we compared our CRLs-based prognostic model with the tumor immune dysfunction and exclusion (TIDE) model and the tumor inflammation signature (TIS) model. Our model showed superior accuracy in predicting the 1-year survival rate of OC samples, with AUC values of 0.629, 0.579, and 0.497 for the CRLs, TIDE, and TIS models, respectively (Figure 5F). In the ICGC cohort, OC patients were also stratified into high-risk and low-risk groups. PCA and t-SNE analysis of the ICGC dataset revealed a clear distinction between high-risk and low-risk components, indicating that the prognostic signature accurately differentiated the two groups (Figure 5G and H). Moreover, the AUC values for 3-year and 5-year survival rates in the ICGC cohort were 0.588 and 0.577, respectively

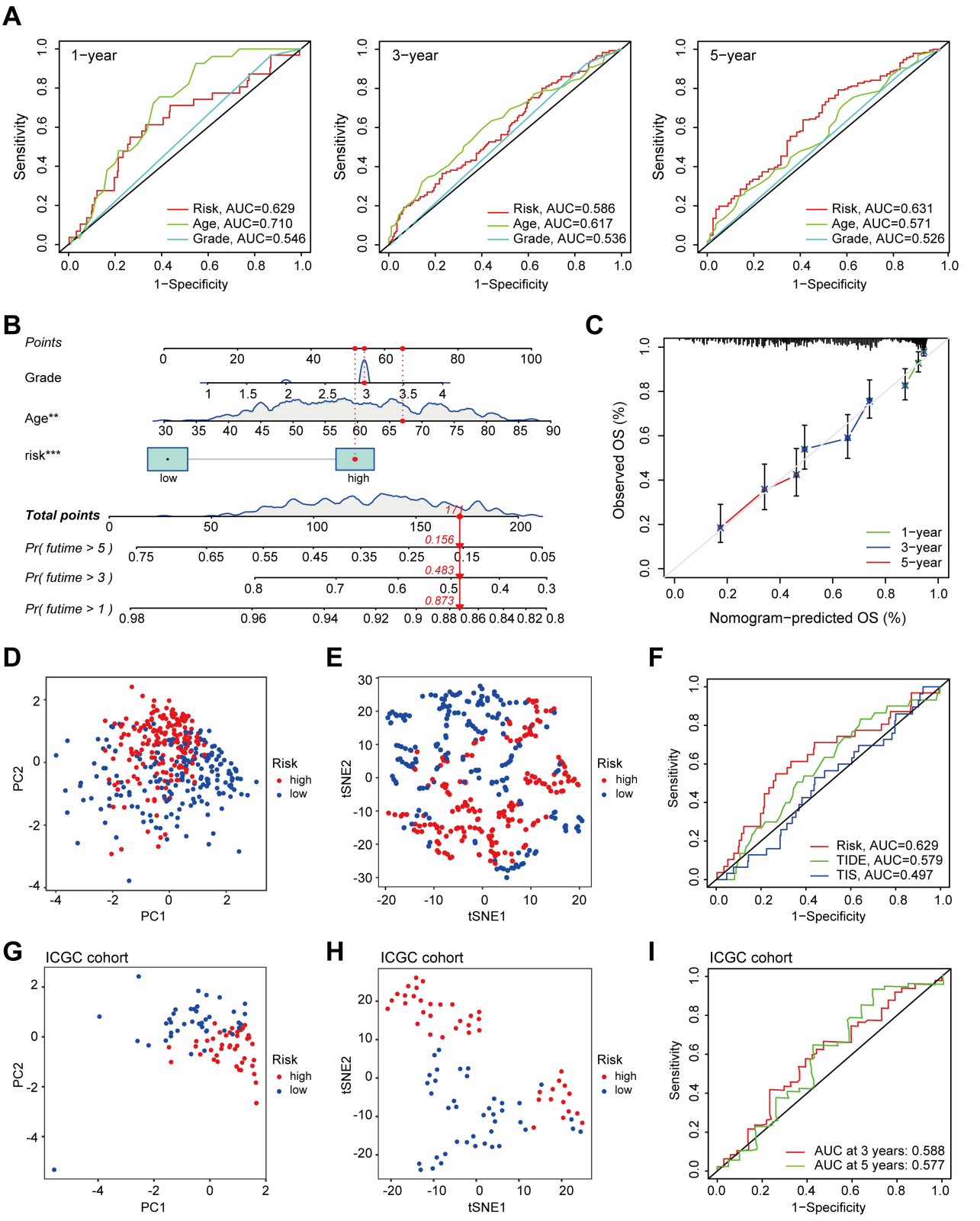

Figure 5 Prognostic Analysis of the 4 CRLs Risk Model in TCGA and ICGC Cohorts. (**A**) ROC curve of 1-, 3-, and 5-year OS for multiple prognostic indicators of OC samples. (**B**) A nomogram combining clinicopathological variables and risk score predicts 1, 3, and 5 years OS of OC patients. (**C**) The calibration curves test consistency between the actual OS rates and the predicted survival rates at 1, 3, and 5 years. (**D**) The PCA plot in the TCGA cohort. (**E**) The t-SNE plot in the TCGA cohort. (**F**) Comparison of the prognostic risk model with TIS models and TIDE models. TIS: Tumor Inflammation Signature; TIDE: Tumor Immune Dysfunction and Exclusion. (**G**) PCA between low-risk and high-risk groups in ICGC cohorts. (**H**) t-SNE analysis of the high-/low-risk groups in the ICGC cohorts. (**I**) 3-year and 5-year ROC curve analysis in ICGC cohorts. *p<0.05, **p<0.01, ***p<0.001.

https://doi.org/10.2147/JIR.S521410

(Figure 5I). Overall, both internal and external validations confirmed the stability and credibility of our CRLs-based prognostic signature in OC.

Pathway Enrichment Analysis of High-/Low-Risk Groups Based on the CRLs Prognostic Signature

To further explore the potential biological pathways and processes associated with different risk levels, we performed Gene Set Variation Analysis (GSVA) and GSEA on the prognostic model genes and risk scores, using the KEGG gene set database. The GSVA results revealed that several critical pathways related to tumorigenesis were significantly enriched in the high-risk group, including the VEGF, WNT, TGF-β, Notch, mTOR, MAPK, Hedgehog, ERBB, and Insulin signaling pathways (Figure 6A). We next analyzed the correlations between the prognostic model genes, risk scores, and immune

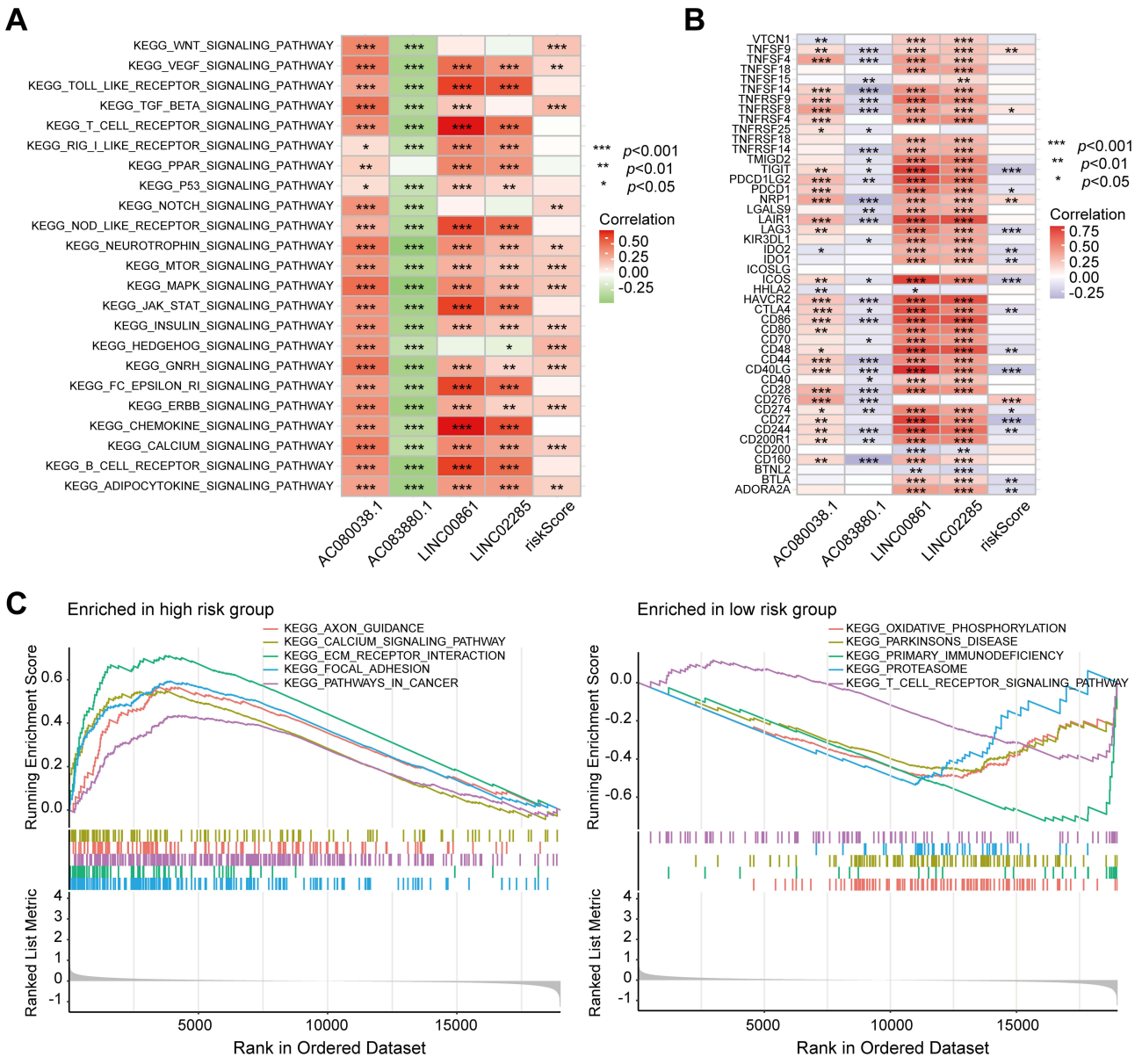

Figure 6 Pathway Enrichment Analysis of High-/Low-Risk Groups Based on the CRLs Prognostic Signature. (**A**) The enrichment of GSVA was used to analyze the correlation between CRLs prognostic signature and signaling pathways. The significance of pathway enrichment in prognostic signature was assessed by the Wilcoxon rank-sum test. (**B**) Heatmap of Spearman correlation analysis between CRLs prognostic signatures and immune checkpoint expression. (**C**) GSEA showed enriched signaling pathways in the high-/low-risk groups of OC patients. *p<0.05, **p<0.01, and ***p<0.001.

https://doi.org/10.2147/JIR.S521410

checkpoints, revealing that most immune checkpoints were negatively associated with the risk scores in OC patients (Figure 6B). Subsequently, GSEA was conducted to explore the biological functions and signaling pathways differing between the high-risk and low-risk groups classified by the 4 CRLs signature. The results indicated that several tumor-related pathways, including ECM receptor interaction and cancer pathways, were enriched in the high-risk group (Figure 6C). In contrast, numerous immune-related pathways, such as primary immunodeficiency and T cell receptor signaling pathways, were enriched in the low-risk group (Figure 6C).

Correlation Analysis Between High/Low-Risk Groups and Immunity

Building on the 6 immunotypes identified in previous studies (C1: wound healing; C2: IFN-γ dominant; C3: inflammatory; C4: lymphocyte depleted; C5: immunologically quiet; C6: TGF-β dominant),[32] we included OC tumor samples with immunogenicity analysis in our study. The results revealed a significant difference in the immunotyping of OC patients between the high-risk and low-risk groups, as determined by a chi-square test (p=0.006). The distribution of immunotypes was predominantly concentrated in C1, C2, and C4 (Figure S2). We then employed various algorithms (TIMER, CIBERSORT, CIBERSORT-ABS, quanTIseq, MCP-counter, xCell, and EPIC) to analyze the immune microenvironment of samples with different risk scores and obtain their immune expression profiles (Figure 7A). To further explore the correlation between risk scores and immune cell infiltration as well as immune functions, we performed a correlation analysis using the GSVA package with ssGSEA. This allowed us to quantify the enrichment scores for various immune cell subgroups, functions, and pathways. The results of immune cell infiltration suggested that infiltration proportions of aDCs, B cells, $CD8^+$ T cells, Mast cells, NK cells, Tfh, Th1 cells, Th2 cells, and TIL were increased in the low-risk group (Figure 7B). As shown in Figure 7C, immunological function shows significant differences between low-/high-risk groups, the results indicated that the immune function scores for cytolytic activity, inflammation promotion, MHC class I, T cell co-inhibition, and T cell co-stimulation were significantly higher in the low-risk group compared to the high-risk group. Similarly, in the ICGC cohort, the level of immune cell infiltration and immune-related functions in the low-risk group were significantly higher than those in the high-risk group (Figure 7D–E), indicating that the low-risk group was related to the protective immune microenvironment. We also examined the differential immune cell survival curves between the high-risk and low-risk groups. KM analysis revealed that high-risk patients with resting memory T cells, activated mast cells, monocytes, and neutrophils had shorter survival compared to low-risk patients. However, high-risk patients with M0 macrophages, M1 macrophages, activated NK cells, plasma cells, follicular helper T cells, gamma-delta T cells, and activated memory $CD4^+$ T cells had longer survival than their low-risk counterparts (Figure S3). Overall, these findings suggest that the risk level in OC patients is associated with immune cell infiltration.

Comparison of Mutation Profiles, TMB, TIDE, MSI, and TME in High-/Low-Risk Groups

Mutation identification plays a crucial role in cancer risk assessment and may inform the development of preventive or therapeutic strategies for OC. We examined somatic mutation distributions between high-risk and low-risk groups and observed the following: in the high-risk group, 121 of 127 samples (95.28%) exhibited mutations, with TP53 and TTN as the top two mutated genes. In the low-risk group, 117 of 129 samples (95.9%) showed mutations, with TP53 and TTN also being the most frequent mutations (Figure 8A). Notably, the high-risk group had a significantly higher rate of TTN mutations compared to the low-risk group, whereas the trend for TP53 mutations was reversed, with a higher mutation rate observed in the low-risk group (Figure 8A).

Tumor mutational burden (TMB) is a key indicator associated with a better response to immune checkpoint blockade (ICB) therapy. Our analysis revealed an inverse correlation between OC patient risk scores and TMB (Figure 8B). Furthermore, mutation data analysis showed that the low-risk group had a higher TMB compared to the high-risk group (Figure 8C), suggesting that low-risk patients may benefit more from immunotherapy. Overall, survival outcomes were better for patients with higher TMB (Figure 8D). A further comparison of TMB between the high-risk and low-risk groups demonstrated that patients in the low-risk group with higher TMB had the best survival probability, while those in the high-risk group with lower TMB had the worst survival probability (Figure 8E). TIDE is a computational framework

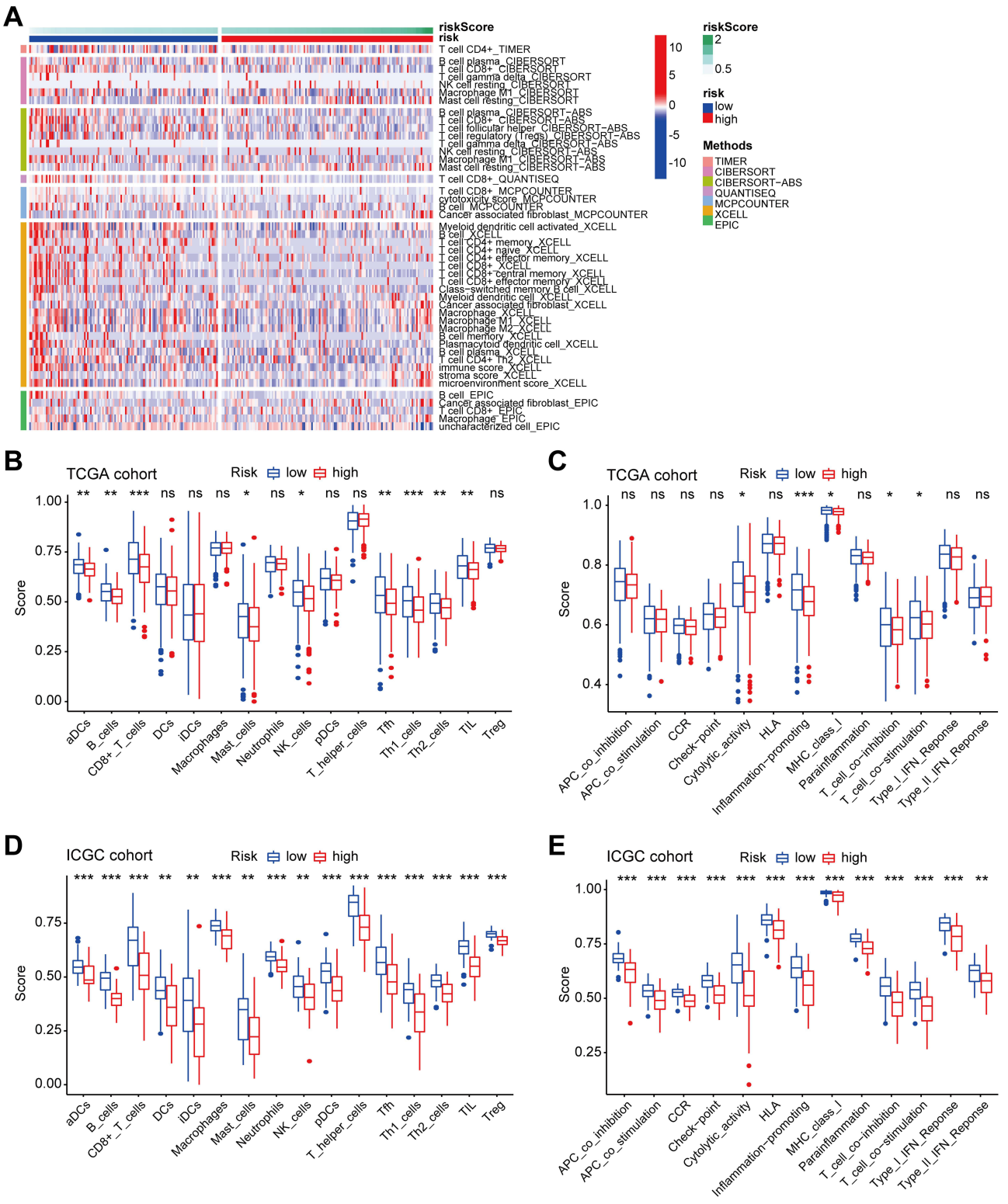

Figure 7 Correlation Analysis Between High/Low-Risk Groups and Immunity. (**A**) A heatmap of all substantially distinct immune cells between the high-risk and low-risk score subgroups. (**B** and **C**) Comparison of the enrichment scores of 16 types of immune cells (**B**) and 13 immune-related pathways (**C**) between low-risk (blue box) and high-risk (red box) groups in the TCGA cohort (**D** and **E**) Comparison of the enrichment scores of 16 types of immune cells (**D**) and 13 immune-related pathways (**E**) between low-risk (blue box) and high-risk (red box) groups in the ICGC cohort. Statistical significance was determined by the Wilcoxon rank-sum test (*p<0.05, **p<0.01, and ***p<0.001).

Abbreviation: ns, no significance.

https://doi.org/10.2147/JIR.S521410

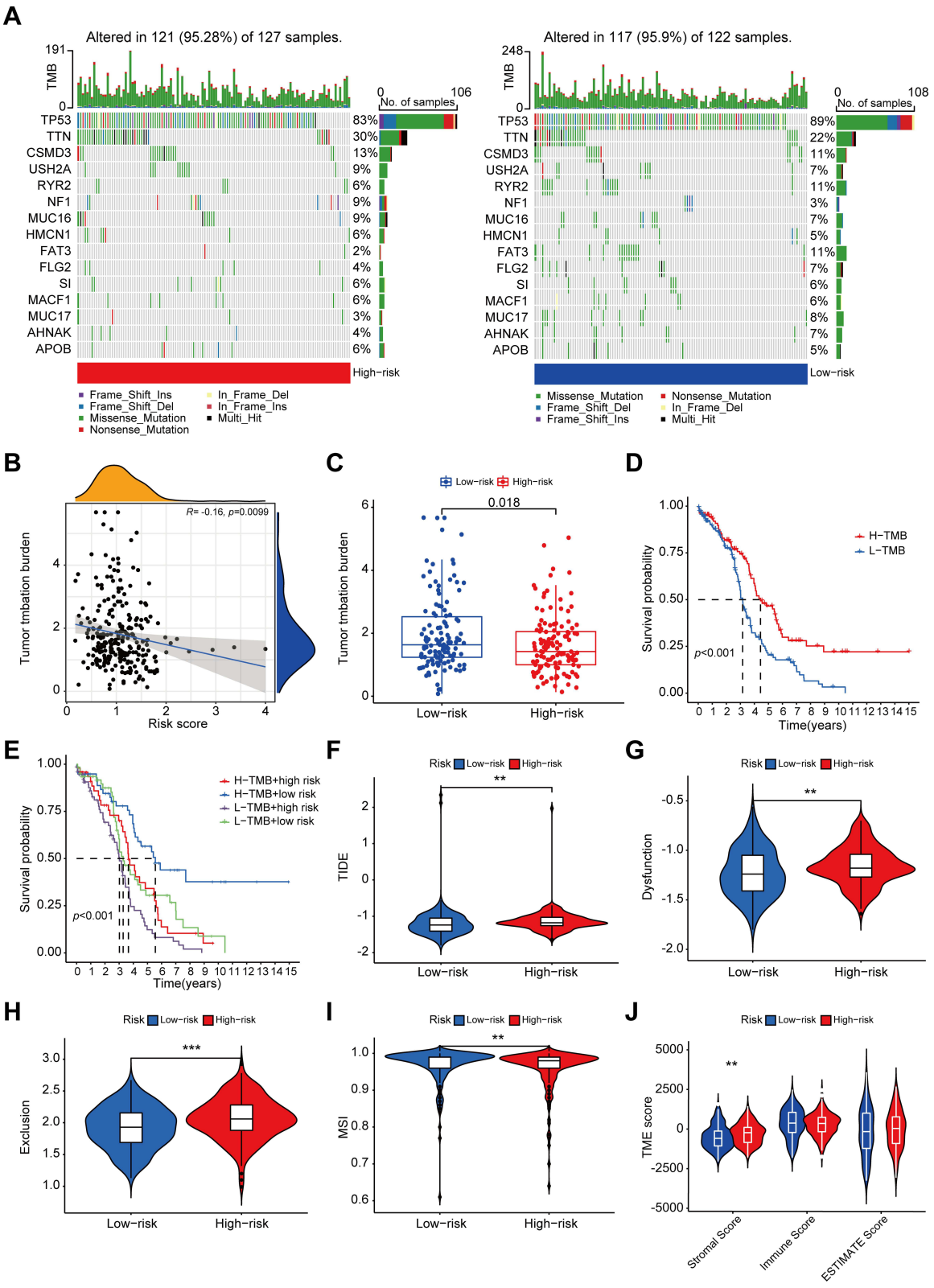

Figure 8 Comparison of Mutation Profiles, TMB, TIDE, MSI, and TME in High-/Low-Risk Groups. (**A**) Heatmap of somatic mutation profile of high-/low-risk individuals. (**B**) Correlation analysis between risk score and TMB. (**C**) The boxplot shows the TMB difference between the high-risk and low-risk groups. (**D**) The KM curves of H-TMB patients and L-TMB patients. (**E**) The KM curves of H-TMB patients and L-TMB patients in the high-/low-risk groups. (**F–I**) Immunotherapy response between high-risk and low-risk groups. Violin plot illuminating the difference of the TIDE score, dysfunction score, exclusion score, and MSI score between the high-risk and low-risk groups. (**J**) Stroma, immune, and ESTIMATE scores in the high-/low-risk groups in OC patients. Statistical significance was assessed using the Wilcoxon rank-sum test. *p<0.05, **p<0.01, and ***p<0.001.

https://doi.org/10.2147/JIR.S521410

that models the two primary mechanisms of tumor immune escape, providing predictive insights into the response to immunotherapy. Given that higher TIDE scores correlate with increased immune evasion and reduced likelihood of benefiting from immune checkpoint inhibitors (ICIs) therapy,[33,34] our analysis revealed that risk scores were positively correlated with TIDE, Dysfunction, and Exclusion scores (Figure 8F–H). Additionally, we investigated the relationship between microsatellite instability (MSI) and the risk groups. The results showed a negative correlation between MSI and risk scores (Figure 8I). To explore differences in immune cell infiltration between the high-risk and low-risk groups, we compared the stromal score (representing substrate cells in tumor tissue), immune score (reflecting immune cell infiltration), and estimate score (the combined sum of stromal and immune scores for individual cases). The analysis revealed that only the stromal score was significantly higher in the high-risk group (Figure 8J).

Immunotherapy Analysis and Drug Sensitivity Prediction in High-/Low-Risk Groups

Several studies have shown that combination therapy with anti-CTLA-4 and anti-PD-1 can enhance the proportion of activated $CD8^+$ T cells and natural killer (NK) cells while reducing the levels of suppressive immune cells in the tumor microenvironment, thereby achieving therapeutic effects against cancer.[35] Building on this, we sought to investigate whether there are differences in immunotherapy responses between high-risk and low-risk groups. To explore this, we downloaded the OC immunotherapy score file from the TCIA database and analyzed the correlation between immunotherapy response predicted by these scores and the risk groups. The results revealed that patients in the low-risk group exhibited a better response to immunotherapy, whether treated with CTLA-4 or PD-1 inhibitors alone or in combination (Figure 9A–D).

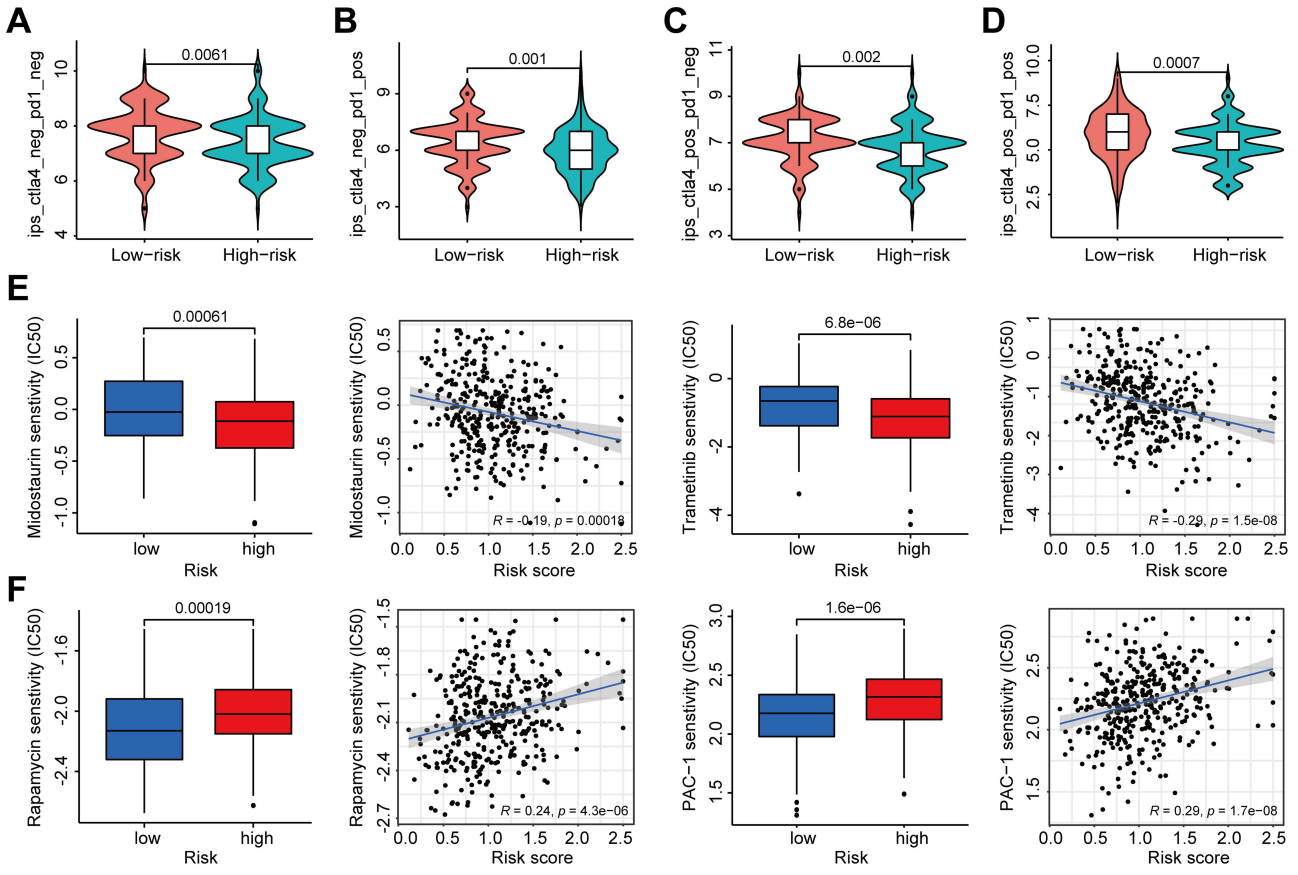

Figure 9 Immunotherapy Analysis and Drug Sensitivity Prediction in High-/Low-Risk Groups. (**A**–**D**) Differences in sensitivity to PD-1 inhibitors, CTLA-4 inhibitors, and the combination of these two inhibitors in different risk score groups. Statistical significance was determined by the Wilcoxon rank-sum test. (**E** and **F**) Boxplot shows the mean differences in estimated IC50 values of 4 representative drugs (Midostaurin, Trametinib, Rapamycin, and PAC-1) between the two risk groups. Lower IC50 indicates higher sensitivity. The Wilcoxon rank-sum test was used. The scatter plot shows the Spearman correlation between the risk score and the drug.

https://doi.org/10.2147/JIR.S521410

Chemotherapy resistance is a significant challenge in the treatment of OC and contributes substantially to cancer mortality. Identifying chemotherapy-sensitive populations could enhance the effectiveness of standard chemotherapy protocols, thereby improving outcomes for OC patients. To investigate the potential for drug resistance between high-risk and low-risk groups, we utilized the "pRRophetic" package to estimate the IC50 values of 251 chemotherapy drugs and inhibitors in both groups. 4 representative drugs are shown in Figure 9E and F. Our analysis suggests that Midostaurin (Multikinase inhibitor) and Trametinib (MEK inhibitor) may demonstrate greater sensitivity in high-risk group patients (Figure 9E), whereas Rapamycin (mTOR inhibitor) and PAC-1 (Procaspase-3 activator) could represent promising therapeutic options for low-risk group patients (Figure 9F).

Exploration of the Expression of CRLs in OC

Building upon the four critical CRLs (AC080038.1, LINC00861, AC083880.1, and LINC02285) identified through our prognostic modeling, we subsequently analyzed their expression profiles between OC tissues and normal tissues in the TCGA database. As illustrated in Figures 10A–D, compared with normal controls, AC080038.1 and LINC00861 exhibited significant downregulation in OC tissues, while AC083880.1 and LINC02285 demonstrated marked upregulation patterns. To validate the reliability of the model, qPCR was performed to verify the expression of the 4 CRLs in normal ovarian cells (IOSE) and OC cells (A2780, SKOV3, and OV90). The expression of AC080038.1 and LINC00861 was lower in OC cells than in normal ovarian cells, whereas that of AC083880.1 and LINC02285 was greater in OC cells than in normal ovarian cells (Figure 10E–H). These results were consistent with our predictions using bioinformatics tools, demonstrating the reliability of the risk model constructed based on the 4 CRLs.

Influence of Abnormal Expression of LINC02285 on Cell Proliferation and Migration in OC

To gain insights into the mechanisms of CRLs in OC, we selected LINC02285 as a representative candidate for in-depth functional characterization in modulating OC progression. LINC02285 was identified as a risk factor (Figure 3C, hazard ratio=2.404) and exhibited significant upregulation in OC tissues compared to normal samples (Figure 10D). At present, no studies have been reported on LINC02285 in OC, so we conducted a series of bioinformatic analyses to evaluate LINC02285. First, we evaluated the prognostic significance of LINC02285 in multiple dataset cohorts via the BEST website (https://rookieutopia.hiplot.com.cn/app_direct/BEST/), analysis confirmed that LINC02285 is an independent

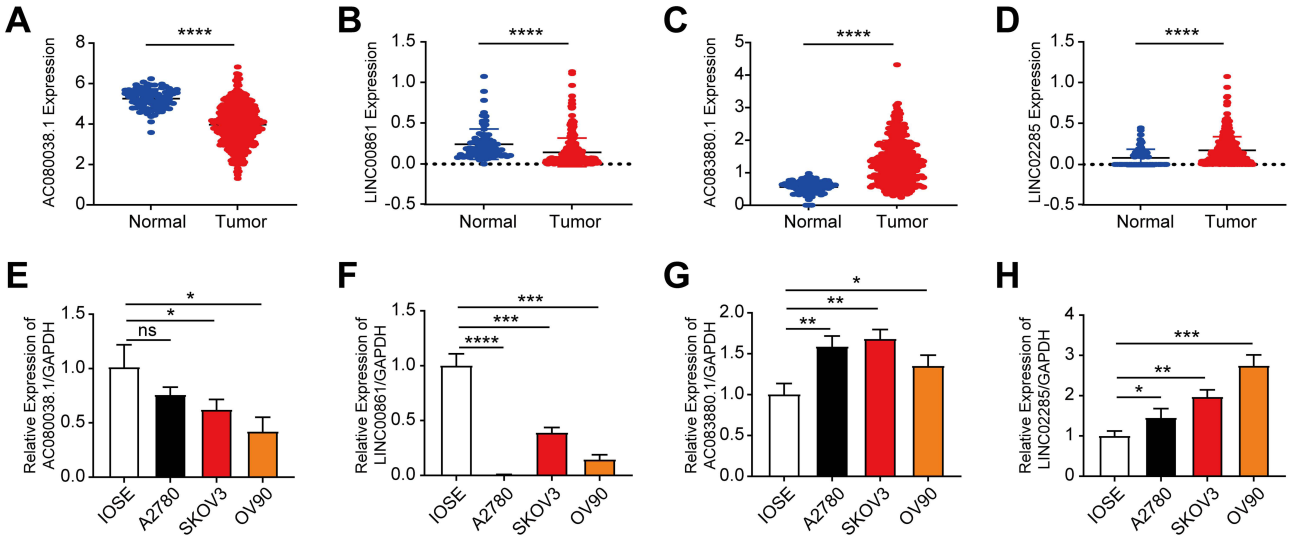

Figure 10 Exploration of the Expression of CRLs in OC. (**A**–**D**) Expression pattern of AC080038.1 (**A**), LINC00861 (**B**), AC083880.1 (**C**), and LINC02285 (**D**) in normal ovarian samples and OC samples in the TCGA+GTEx database. (**E**–**H**) qPCR was used to detect the expression of AC080038.1 (**E**), LINC00861 (**F**), AC083880.1 (**G**), and LINC02285 (**H**) expression in normal ovarian cells (IOSE) and OC cells (A2780, SKOV3, and OV90). In all statistical plots, data are expressed as the mean ± SD. *p<0.05, **p<0.01, ***p<0.001, ****p<0.0001.

prognostic factor in OC, and high expression of LINC02285 in OC patients is closely associated with poor prognosis (Figure S4A). Furthermore, survival analysis from the BEST website also revealed that high expression of LINC02285 was associated with poorer OS outcomes in the GSE73614 dataset (Figure S4B). The high expression of LINC02285 was positively correlated with more lymphatic invasion (Figure S4C) and venous invasion (Figure S4D). Similarly, the UALCAN website (https://ualcan.path.uab.edu/) revealed that LINC02285 expression increases with the advancing OC patients' age, grade, and stage (Figure S4E–G).

Then, to elucidate the functional role of LINC02285 on OC progression, we constructed an overexpressed plasmid of LINC02285 (LINC02285-OE) in PCDH empty-vector to enhance the expression of LINC02285 in OC cell lines. The qPCR results showed that LINC02285 was significantly upregulated in both A2780 and SKOV3 cells (Figures 11A and S5A), suggesting successful transfection of the overexpressed plasmid into OC cells. The fluorescence results are shown in the Figures 11B and S5B. The colony formation assay indicated that overexpression of LINC02285 significantly promoted OC cell growth (Figures 11C and S5C). Transwell and wound healing assays then demonstrated that LINC02285-OE strongly

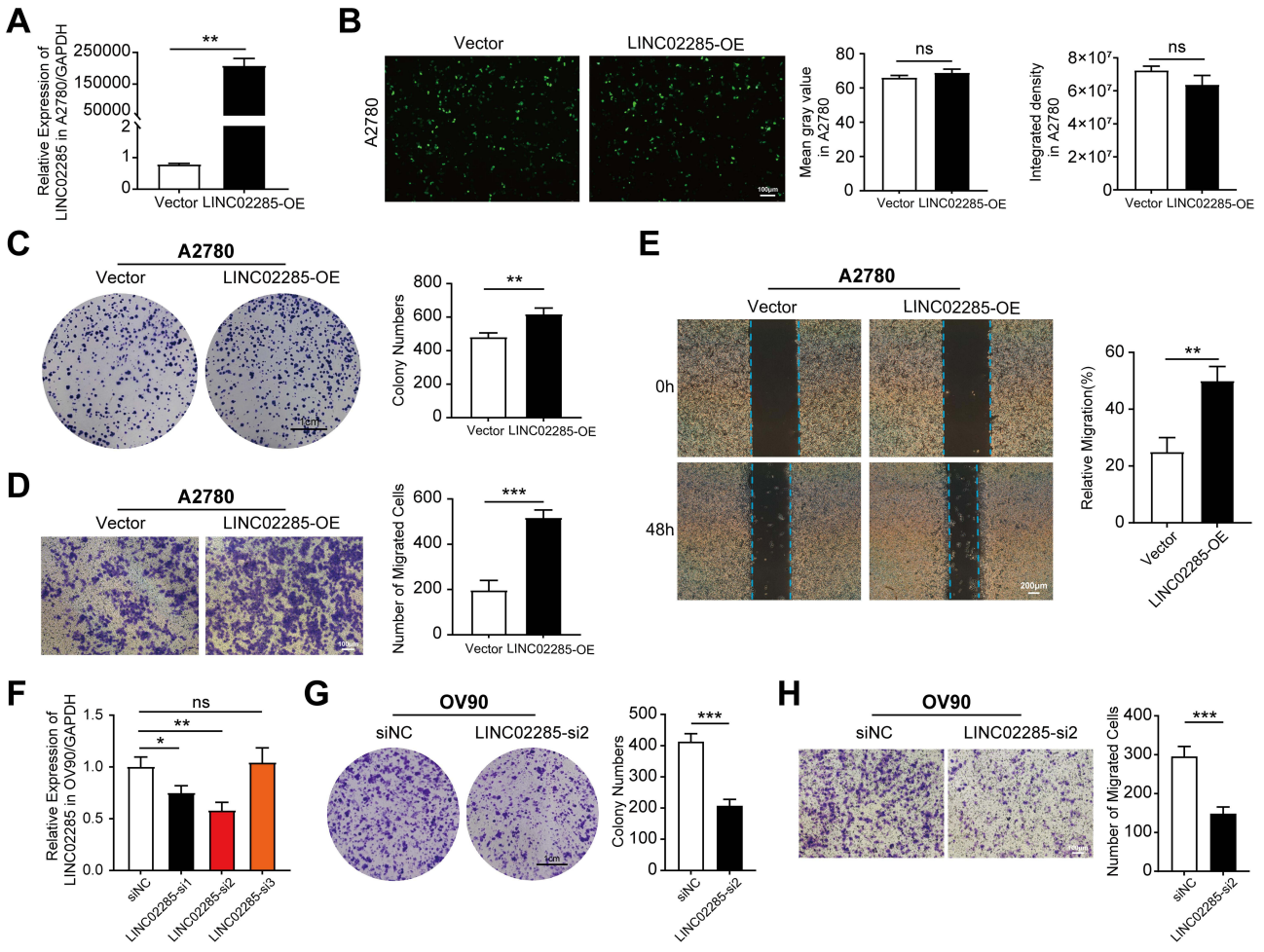

Figure 11 Influence of Abnormal Expression of LINC02285 on Cell Proliferation and Migration in OC. (**A**) Validation of LINC02285 expression after transfection of LINC02285-OE and empty-vector (PCDH) plasmids in A2780 cells using qPCR. GAPDH was used for endogenous controls. (**B**) The effectiveness of the LINC02285-OE and empty-vector (PCDH) plasmids with GFP fluorescence in A2780 cells were detected using a fluorescence microscope (left, Scale bars: 100 μm), the quantized figure is the Mean gray value (middle) and Integrated density (right). (**C**) The colony formation assay displays the effect of LINC02285 upregulation on A2780 cells proliferation ability. (**D–E**) The effects of LINC02285-OE on A2780 cells migration were evaluated through Transwell (**D**) and wound healing (**E**) assays. (**F**) The transfection efficiency of LINC02285 siRNA in OV90 was detected by qPCR. (**G**) Knockdown of LINC02285 inhibited the proliferation ability of OV90 cells and was evaluated by a colony formation assay. (**H**) Transwell assays were performed to determine the effect of LINC02285 knockdown on the migration ability of OV90 cells. All the experiments were performed in triplicate. In all statistical plots, data are expressed as the mean ± SD, revealed by an unpaired two-tailed *t*-test. **p*<0.05, ***p*<0.01, ****p*<0.001, ns: no significance.
Abbreviation: ns, no significance.

https://doi.org/10.2147/JIR.S521410

promoted cell migration capability in vitro (Figures 11D, E, S5D and E). These results implied the involvement of LINC02285 in the proliferation and migration of OC cells, highlighting its potential role in promoting OC progression.

We next selectively knocked down LINC02285 in OV90 cells using siRNA. The siRNA construct LINC02285-si2 was chosen for subsequent assays due to its effective knockdown efficiency (Figure 11F). To assess the impact of LINC02285 knockdown on cell proliferation, we performed colony formation assays in OV90 cells with or without LINC02285 knockdown. The results showed that compared with the siNC control group, the proliferation rate was significantly decreased after LINC02285 knockdown (Figure 11G). We also examined the effect of LINC02285 knockdown on cell migration using Transwell assays. The results revealed a marked reduction in the migratory ability of OC cells upon inhibition of LINC02285 expression (Figure 11H). Collectively, these findings suggest that silencing LINC02285 expression inhibits both the proliferation and migration of OC cells.

LINC02285 Is Associated with Copper Ionophore-Induced Cell Death

Elesclomol is a copper-binding small molecule and Elesclomol-induced cell death results from the accumulation of intracellular copper rather than from the direct effects of Elesclomol itself.[36,37] However, the mechanisms underlying copper-induced cytotoxicity in OC cells remain elusive. To investigate this, we first determined the IC50 of Elesclomol-$CuCl_2$ (1: 1) in A2780 cells following 24 h treatment, which was calculated to be 18 nM (Figure 12A). To investigate cuproptosis induction, we established an experimental model comprising three groups: negative control (NC), Elesclomol-$CuCl_2$ (18 nM, 1:1, 24 h treatment), and TTM-Elesclomol-$CuCl_2$ (pretreated with 20 μM tetrathiomolybdate (TTM), a copper chelator, followed by 18 nM Elesclomol-$CuCl_2$). Notably, TTM restored A2780 cell viability under Elesclomol-$CuCl_2$-induced conditions (Figure 12B), confirming the copper-dependent nature of this cell death mechanism. We then examined whether LINC02285 overexpression modulates cuproptosis by comparing OC cell viability recovery between Vector and LINC02285-OE groups following Elesclomol-$CuCl_2$ treatment. The results revealed a significant difference in cell viability between the two groups after 24 h of Elesclomol-$CuCl_2$ treatment,

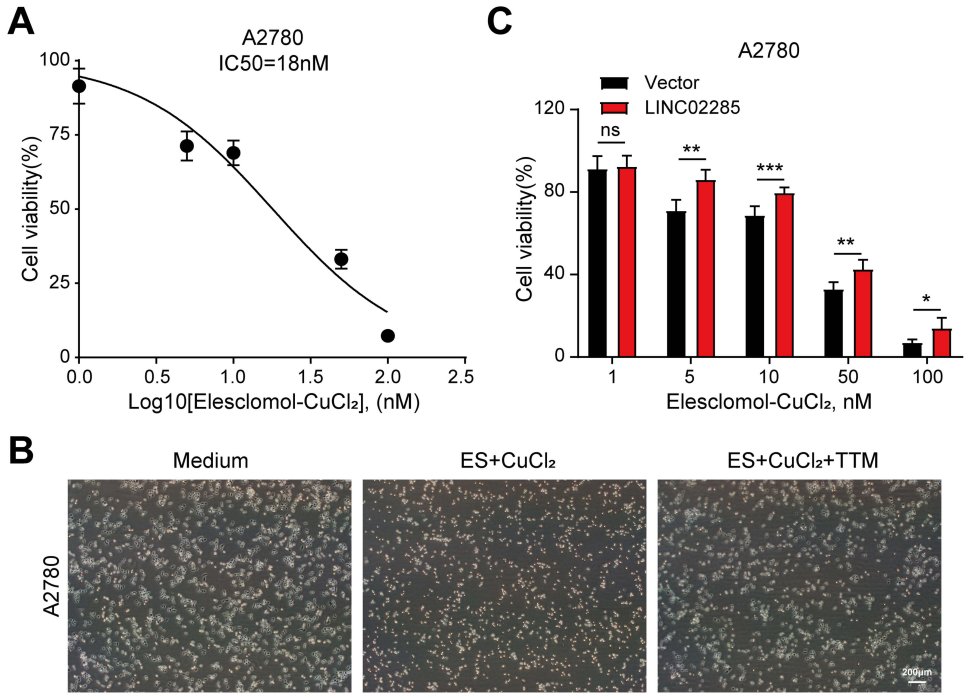

Figure 12 LINC02285 is Associated with Copper Ionophore-Induced Cell Death. (**A**) A2780 cells were exposed to different doses of Elesclomol-$CuCl_2$ for 24 h and detected by CCK-8 assay. (**B**) Representative images of A2780 cells treated with Elesclomol-$CuCl_2$ with or without TTM for 24 h. Scale bars represent 200 μm. (**C**) A2780 cells transfected with LINC02285-OE were treated with various concentrations of elesclomol for 24 h. Cell viability was evaluated by CCK-8 assay. In all statistical plots, data are expressed as the mean ± SD. *p<0.05, **p<0.01, ***p<0.001, ns: no significance.
Abbreviation: ns, no significance.

with the LINC02285-OE group showing markedly higher viability than the Vector group (Figure 12C). These findings indicate that LINC02285-OE enhances the ability of OC cells to restore viability following Elesclomol-$CuCl_2$ treatment. In conclusion, LINC02285-OE mitigates copper-induced cell death in OC cells treated with Elesclomol-$CuCl_2$.

Discussion

Rising global cancer incidence rates have attracted widespread attention, the traditional treatment methods for ovarian cancer (OC) mainly include cytoreductive surgery and chemotherapy regimens based on platinum drugs, yet the prognosis for patients remains grim.[38–40] This stark clinical reality underscores the urgent need for prognostic models. Biomarkers play a pivotal role in precision medicine for OC, serving not only for early detection and prognosis evaluation but also providing crucial guidance for personalized treatment strategies. For instance, BRCA1/2 gene mutations and homologous recombination deficiency (HRD) represent important therapeutic targets in advanced OC.[41] Additionally, while commonly used biomarkers like CA125 and HE4 are valuable, their limited sensitivity and specificity in early detection often necessitate combination with other biomarkers to improve diagnostic accuracy.[3–5] Consequently, identifying effective therapeutic targets remains paramount for both diagnosis and treatment of OC.

Cuproptosis, as a novel cellular death mechanism, has become a hot topic of research in recent years.[42,43] An increasing body of evidence suggests that copper homeostasis is closely linked to the development of various tumors, with its dysregulation influencing cancer cell growth and proliferation through cytotoxic effects.[44,45] Cuproptosis, an unconventional form of cell death associated with protein lipoylation in the TCA cycle, offers novel potential for leveraging copper toxicity in cancer treatment.[46–48] In the field of lncRNA, CRLs are also increasingly becoming the focus of research. Several studies have used CRLs to construct predictive signatures for cancer prognosis.[49–51] Although there is growing interest in the potential connection between CRLs and OC, there is currently no direct experimental or clinical evidence to support such a link.

In this study, we aim to construct the CRLs signature-based prognostic prediction model to evaluate OC patients' overall survival and its correlation with tumor immune activity, mutational status, and chemotherapy response. During model construction, variable selection represents a critical step—the inclusion of excessive lncRNAs may lead to overfitting issues, thereby compromising the predictive accuracy of risk scores.[52] To address this, the following analytical workflow was implemented: first, four prognosis-associated lncRNAs (AC080038.1, AC083880.1, LINC00861, and LINC02285) were preliminarily screened through univariate Cox regression; subsequently, multivariate Cox regression combined with LASSO regression analysis ultimately identified these four CRLs as core components of the predictive signature. The risk score for each patient was calculated using the established formula, and the OC patients were categorized into high-risk and low-risk groups based on the median value. The OS time in the high-risk group was markedly shorter than that in the low-risk group. The ROC curve analysis demonstrated that the predictive signature exhibited strong performance in risk stratification. Subsequently, the risk score was combined with clinical factors (such as age and grade) to develop a predictive nomogram, improving its practical utility and clinical applicability. Both PCA and t-SNE analyses revealed distinct separation between the high-risk and low-risk groups, indicating the model's ability to accurately distinguish between them. Similarly, the reliability of the predictive signature was confirmed through both internal and external validation.

Recent studies have increasingly highlighted the role of lncRNAs in modulating the tumor immune microenvironment, particularly their impact on infiltrating immune cells, where they have been shown to play significant roles in various cancer types.[53–55] Functional analyses revealed that the differentially expressed CRLs between the high-risk and low-risk groups were associated with immune-related pathways. A comparison of immune cell infiltration and pathway activation between these groups showed that the high-risk group exhibited generally lower levels of immune cell infiltration and reduced activity of immune-related pathways compared to the low-risk group. Based on these findings, the poor survival outcomes observed in high-risk OC patients may be attributed to reduced levels of antitumor immunity. Numerous studies have shown that patients with a high TMB, due to their greater number of neoantigens, may benefit more from immunotherapy.[56–58] Our analysis of mutational data revealed that high-risk patients exhibited significantly lower TMB compared to low-risk patients, suggesting potentially greater benefit from immunotherapy in low-risk

individuals. Similarly, we observed markedly higher TIDE scores in the high-risk patient cohort, suggesting a more active tumor immune escape mechanism within their tumor microenvironment.

Additionally, we analyzed the differences in sensitivity to PD-1 and CTLA-4 inhibitors between high-risk and low-risk OC patients using data from the TCIA database. Our results revealed that low-risk patients exhibited significantly higher sensitivity to PD-1 inhibitors (p=0.001), CTLA-4 inhibitors (p=0.002), and the combination of PD-1 and CTLA-4 inhibitors (p=0.0007). These findings suggest that immune checkpoint inhibitors (ICIs) therapy could be a potential treatment option for OC patients. Consistent with existing studies, the combination of CTLA-4 and PD-1 inhibitors may enhance the efficacy of immunotherapy in OC.[59] Notably, when combined with chemotherapy, anti-angiogenic agents, PARP inhibitors, or antibody-drug conjugates (ADCs), these combination therapies exhibit significant synergistic effects that may improve survival outcomes in OC patients.[59]

On the other hand, high-risk OC patients may be more responsive to chemotherapy drugs such as Midostaurin and Trametinib. Research evidence indicates that neoadjuvant chemotherapy (NACT) combined with interval debulking surgery (IDS) offers significant advantages in the treatment of advanced OC. This therapeutic approach not only effectively reduces tumor burden and decreases surgical difficulty but also improves the resection rate, lowers the incidence of postoperative complications, and enhances patients' quality of life. However, microscopic residual disease (MRD) remains a critical prognostic factor, particularly during IDS, where complete eradication of potential MRD is essential for improving long-term survival.[60] Consequently, the key to optimizing the NACT-IDS strategy in the future lies in further reducing MRD, with potential measures including increasing the number of chemotherapy cycles or utilizing more precise imaging assessment methods (such as MRI or PET-CT) to refine surgical decision-making. Therefore, for high-risk OC patients, molecularly-guided personalized treatment may provide additional clinical benefits. For instance, targeted agents such as Midostaurin (Multikinase inhibitor) or Trametinib (MEK inhibitor) combined with the NACT-IDS strategy could potentially enhance tumor cell-killing efficacy through synergistic effects, thereby more effectively eliminating MRD. This combination approach may demonstrate potential advantages in reducing postoperative residual lesions, delaying recurrence, and improving survival rates. However, its clinical value still requires further validation through prospective studies to establish optimal treatment regimens and confirm long-term therapeutic outcomes.

To further understand the mechanism of action of CRLs in OC, we confirmed the differential expression of these CRLs in OC cells and normal ovarian cells by qPCR assay and revealed the effect of risk factor LINC02285 on the proliferation and migration of OC cells by cell function assay. Furthermore, we identified an association between LINC02285 and copper ionophore-induced cell death. Notably, LINC02285 overexpression attenuated copper-induced cell death in OC cells treated with Elesclomol-$CuCl_2$. These results suggest that LINC02285, the first lncRNA demonstrated to promote tumor survival by inhibiting cuproptosis in OC, may represent a novel therapeutic target for OC patients. Current evidence has established that LINC02285 promotes tumor progression via PI3K-AKT signaling pathway regulation and demonstrates potential as a prognostic biomarker.[61] Nevertheless, the mechanism of LINC02285in the regulation of the tumor immune microenvironment has not yet been clarified, which will be an important direction for future research.

Among the other 3 lncRNAs (AC080038.1, AC083880.1, and LINC00861) included in the prognostic model, functional enrichment analysis revealed that AC080038.1 participates in gastric cancer-associated cellular metabolic reprogramming and immune regulation through ceRNA networks, providing mechanistic support for its role as a novel prognostic biomarker.[62] While the results are promising, they necessitate further experimental validation and larger cohort studies for confirmation and refinement. Notably, bioinformatics analysis demonstrated AC083880.1's close association with immune modulation, suggesting its potential as a prognostic target in pancreatic cancer.[63] However, more experiments are needed to clarify this mechanism. Moreover, LINC00861 has been identified as a hub lncRNA in various cancers, participating in various immune-related pathways.[64–66] These findings suggest that LINC00861 may regulate immune cell infiltration through modulating the expression of immune-associated genes. Although the role of LINC00861 in multiple cancers has been preliminarily verified, its specific molecular mechanism still requires further in-depth study. Given their established involvement in immune-related pathways and prognostic value in other

malignancies, systematic investigation of these lncRNAs in OC tumor immunology represents a critical research frontier with potential therapeutic implications.

However, there are several limitations to our study. One of the limitations is that the major part of the cohort in this study is derived from the TCGA and ICGC databases, which are retrospective studies and need to be validated by prospective analysis. The other limitation is that the molecular mechanisms underlying the risk model remain to be fully elucidated. Although we identified the key risk factor LINC02285 as potentially involved in the cuproptosis process of OC, the specific molecular mechanisms behind this association require further validation through additional in vitro and in vivo experiments. To further verify the feasibility of the prediction model and its potential mechanism, we will collect more samples and perform experiments. Despite these limitations, the identification of LINC02285 as a potential novel biomarker for OC through bioinformatics analysis and preliminary experimental validation provides valuable insights for future investigations into OC pathogenesis and the development of therapeutic strategies.

In conclusion, this study highlights the crucial role of CRLs in the prognostic model for OC. The prognostic risk score, derived from the expression signature of CRLs, demonstrated strong predictive performance for both OS and PFS in OC patients and was significantly associated with immune cell infiltration levels and immune-related functions. Moreover, high expression of the LINC02285 was associated with poor prognosis and an immunosuppressive tumor microenvironment, suggesting its potential as both a prognostic biomarker and a therapeutic target for OC.

Conclusions

In summary, we constructed an accurate prognostic signature consisting of four CRLs. The signature serves as a new biomarker to assess distinct OS, immune cell level in the tumor microenvironment, TMB, the potential immunotherapeutic benefits, and chemotherapeutic sensitivity for OC patients. Besides, we discovered that LINC02285 overexpression was shown to enhance the proliferative and migratory capacities of OC cells while conferring resistance to copper-induced cell death. These findings shed light on the roles of CRLs in clinical implications and progression of OC. This signature can aid clinicians in identifying specific patient subgroups who may benefit from personalized immunotherapy and chemotherapy.

Abbreviations

OC, Ovarian Cancer; CRGs, Cuproptosis-Related Genes; CRLs, Cuproptosis-Related LncRNAs; OS, Overall Survival; TCA, Tricarboxylic Acid; LncRNAs, Long noncoding RNAs; GSEA, Gene Set Enrichment Analysis; TCGA, The Cancer Genome Atlas; ICGC, International Cancer Genome Consortium; CNV, Copy Number Variation; TIMER, Tumor Immune Estimation Resource; KM, Kaplan Meier; PCA, Principal Component Analysis; t-SNE, t-distributed Stochastic Neighbor Embedding; LASSO, Least Absolute Shrinkage and Selection Operator; ROC, Receiver Operating Characteristic; KEGG, Kyoto Encyclopedia of Genes and Genomes; ssGSEA, single sample Gene Set Enrichment Analysis; TMB, Tumor Mutation Burden; TIDE, Tumor Immune Dysfunction and Exclusion; TCIA, The Cancer Immunome Atlas; ICIs, Immune Checkpoint Inhibitors; IC50, Inhibitory Concentration 50; DEGs, Differentially Expressed Genes; ICB, Immune Checkpoint Blockade; TIS, Tumor Inflammation Signature; GSVA, Gene Set Variation Analysis; IDS, Interval Debulking Surgery; NACT, Neoadjuvant Chemotherapy; MRD, Microscopic Residual Disease.

Data Sharing Statement

All data generated or analyzed during the study period were included in this published article and its Supplementary Information. Publicly available datasets were analyzed in this study. This data can be found here: The datasets analyzed in the current study are available in the TCGA repository (https://portal.gdc.cancer.gov/), GTEx website (https://www.gtexportal.org/), UCSC Xena (https://xenabrowser.net/), ICGC database (https://icgc.org), and TCIA database (https://tcia.at/). The datasets used and/or analyzed during the current study are available from the corresponding author upon reasonable request.

Ethics Approval and Informed Consent

The present study was approved by the Ethics Committee of Xiangya School of Basic Medical Science, Central South University (2025-KT128).

Acknowledgments

All authors express their profound gratitude to the developers of the public databases utilized in this study. We appreciate the support of all people involved in the present study and thank Central South University for its support of the Student Innovation Project.

Author Contributions

All authors made a significant contribution to the work reported, whether that is in the conception, study design, execution, acquisition of data, analysis and interpretation, or in all these areas; took part in drafting, revising or critically reviewing the article; gave final approval of the version to be published; have agreed on the journal to which the article has been submitted; and agree to be accountable for all aspects of the work.

Funding

This research was funded by the National Natural Science Foundation of China grant numbers 82173376 and 82372711, and the Student Innovation Project of Central South University grant number 2023ZZTS0845.

Disclosure

The authors report no conflicts of interest in this work.

References

1. Bray F, Laversanne M, Sung H, et al. Global cancer statistics 2022: GLOBOCAN estimates of incidence and mortality worldwide for 36 cancers in 185 countries. *CA Cancer J Clinicians*. 2024;74(3):229–263. doi:10.3322/caac.21834
2. Siegel RL, Giaquinto AN, Jemal A. Cancer statistics, 2024. *CA Cancer J Clinicians*. 2024;74(1):12–49. doi:10.3322/caac.21820
3. Zhang M, Cheng S, Jin Y, Zhao Y, Wang Y. Roles of CA125 in diagnosis, prediction, and oncogenesis of ovarian cancer. *Biochim Biophys Acta Rev Cancer*. 2021;1875(2):188503. doi:10.1016/j.bbcan.2021.188503
4. Anastasi E, Farina A, Granato T, et al. Recent Insight about HE4 role in ovarian cancer oncogenesis. *Int J Mol Sci*. 2023;24(13):10479. doi:10.3390/ijms241310479
5. Song Y, Yuan M, Wang G. Update value and clinical application of MUC16 (cancer antigen 125). *Expert Opin Ther Targets*. 2023;27(8):745–756. doi:10.1080/14728222.2023.2248376
6. Atakul T, Altinkaya SO, Abas BI, Yenisey C. Serum copper and zinc levels in patients with Endometrial Cancer. *Biol Trace Elem Res*. 2020;195(1):46–54. doi:10.1007/s12011-019-01844-x
7. Ressnerova A, Raudenska M, Holubova M, et al. Zinc and copper homeostasis in head and neck cancer: review and meta-analysis. *Curr Med Chem*. 2016;23(13):1304–1330. doi:10.2174/0929867323666160405111543
8. Tsvetkov P, Coy S, Petrova B, et al. Copper induces cell death by targeting lipoylated TCA cycle proteins. *Science*. 2022;375(6586):1254–1261. doi:10.1126/science.abf0529
9. Ge EJ, Bush AI, Casini A, et al. Connecting copper and cancer: from transition metal signalling to metalloplasia. *Nat Rev Cancer*. 2022;22(2):102–113. doi:10.1038/s41568-021-00417-2
10. Yan T, Yang H, Meng Y, et al. Targeting copper death genotyping associated gene RARRES2 suppresses glioblastoma progression and macrophages infiltration. *Cancer Cell Int*. 2023;23(1):105. doi:10.1186/s12935-023-02950-6
11. Babak MV, Ahn D. Modulation of intracellular copper levels as the mechanism of action of anticancer copper complexes: clinical relevance. *Biomedicines*. 2021;9(8):852. doi:10.3390/biomedicines9080852
12. Wang L, Li Y, Wang Y, et al. Identification of cuproptosis-related lncRNAs for prognosis and immunotherapy in glioma. *J Cell Mol Med*. 2022;26(23):5820–5831. doi:10.1111/jcmm.17603
13. Xu M, Mu J, Wang J, Zhou Q, Wang J. Construction and validation of a cuproptosis-related lncRNA signature as a novel and robust prognostic model for colon adenocarcinoma. *Front Oncol*. 2022;12:961213. doi:10.3389/fonc.2022.961213
14. Xiong J, Wu L, Huang L, et al. LncRNA FOXP4-AS1 promotes progression of ewing sarcoma and is associated with immune infiltrates. *Front Oncol*. 2021;11:718876. doi:10.3389/fonc.2021.718876
15. Han G, Guo Q, Ma N, et al. LncRNA BCRT1 facilitates osteosarcoma progression via regulating miR-1303/FGF7 axis. *Aging*. 2021;13(11):15501–15510. doi:10.18632/aging.203106
16. Li J, Meng H, Bai Y, Wang K. Regulation of lncRNA and its role in cancer metastasis. *Oncology Research*. 2016;23(5):205–217. doi:10.3727/096504016x14549667334007
17. Peng WX, Koirala P, Mo YY. LncRNA-mediated regulation of cell signaling in cancer. *Oncogene*. 2017;36(41):5661–5667. doi:10.1038/onc.2017.184

18. Liu L, Wang Q, Zhou JY, Zhang B. Developing four cuproptosis-related lncRNAs signature to predict prognosis and immune activity in ovarian cancer. *J Ovarian Res*. 2023;16(1):88. doi:10.1186/s13048-023-01165-7
19. Kuang M, Liu Y, Chen H, et al. Big data analysis and machine learning of the role of cuproptosis-related long non-coding RNAs (CuLncs) in the prognosis and immune landscape of ovarian cancer. *Front Immunol*. 2025;16:1555782. doi:10.3389/fimmu.2025.1555782
20. Chen R, Huang Y, Sun K, et al. Construction of a prognostic model for ovarian cancer based on a comprehensive bioinformatics analysis of cuproptosis-associated long non-coding RNA signatures. *Heliyon*. 2024;10(15):e35004. doi:10.1016/j.heliyon.2024.e35004
21. Wang Y, Liang Q, Xu L, et al. Cuproptosis-related lncRNAs ovarian cancer: multi-omics analysis of molecular mechanisms and potential therapeutic targets. *Environ Toxicol*. 2024;39(3):1650–1665. doi:10.1002/tox.24067
22. Mayakonda A, Lin DC, Assenov Y, Plass C, Koeffler HP. Maftools: efficient and comprehensive analysis of somatic variants in cancer. *Genome Res*. 2018;28(11):1747–1756. doi:10.1101/gr.239244.118
23. Goldman MJ, Craft B, Hastie M, et al. Visualizing and interpreting cancer genomics data via the Xena platform. *Nature Biotechnol*. 2020;38 (6):675–678. doi:10.1038/s41587-020-0546-8
24. Blockhuys S, Celauro E, Hildesjö C, et al. Defining the human copper proteome and analysis of its expression variation in cancers. *Metallomics*. 2017;9(2):112–123. doi:10.1039/c6mt00202a
25. Wang Y, Zhang L, Zhou F. Cuproptosis: a new form of programmed cell death. *Cell Mol Immunol*. 2022;19(8):867–868. doi:10.1038/s41423-022-00866-1
26. Newman AM, Liu CL, Green MR, et al. Robust enumeration of cell subsets from tissue expression profiles. *Nature Methods*. 2015;12(5):453–457. doi:10.1038/nmeth.3337
27. Klempner SJ, Fabrizio D, Bane S, et al. Tumor mutational burden as a predictive biomarker for response to immune checkpoint inhibitors: a review of current evidence. *Oncologist*. 2020;25(1):e147–e159. doi:10.1634/theoncologist.2019-0244
28. Jiang P, Gu S, Pan D, et al. Signatures of T cell dysfunction and exclusion predict cancer immunotherapy response. *Nature Med*. 2018;24 (10):1550–1558. doi:10.1038/s41591-018-0136-1
29. Geeleher P, Cox N, Rs H. pRRophetic: an R package for prediction of clinical chemotherapeutic response from tumor gene expression levels. *PLoS One*. 2014;9(9):e107468. doi:10.1371/journal.pone.0107468
30. Robinson AG, Booth CM, Eisenhauer EA. Progression-free survival as an end-point in solid tumours--perspectives from clinical trials and clinical practice. *Eur J Cancer*. 2014;50(13):2303–2308. doi:10.1016/j.ejca.2014.05.024
31. Pasalic D, McGinnis GJ, Fuller CD, et al. Progression-free survival is a suboptimal predictor for overall survival among metastatic solid tumour clinical trials. *Eur J Cancer*. 2020;136:176–185. doi:10.1016/j.ejca.2020.06.015
32. Thorsson V, Gibbs DL, Brown SD, et al. The immune landscape of cancer. *Immunity*. 2018;48(4):812–830.e814. doi:10.1016/j.immuni.2018.03.023
33. Chen Y, Li ZY, Zhou GQ, Sun Y. An immune-related gene prognostic index for head and neck squamous Cell carcinoma. *Clin Cancer Res*. 2021;27 (1):330–341. doi:10.1158/1078-0432.Ccr-20-2166
34. Wu J, Li L, Zhang H, et al. A risk model developed based on tumor microenvironment predicts overall survival and associates with tumor immunity of patients with lung adenocarcinoma. *Oncogene*. 2021;40(26):4413–4424. doi:10.1038/s41388-021-01853-y
35. Reardon DA, Gokhale PC, Klein SR, et al. Glioblastoma eradication following immune checkpoint blockade in an orthotopic, immunocompetent model. *Cancer Immunol Res*. 2016;4(2):124–135. doi:10.1158/2326-6066.Cir-15-0151
36. Buccarelli M, D'Alessandris QG, Matarrese P, et al. Elesclomol-induced increase of mitochondrial reactive oxygen species impairs glioblastoma stem-like cell survival and tumor growth. *J Exp Clin Cancer Res*. 2021;40(1):228. doi:10.1186/s13046-021-02031-4
37. Gao W, Huang Z, Duan J, et al. Elesclomol induces copper-dependent ferroptosis in colorectal cancer cells via degradation of ATP7A. *Mol Oncol*. 2021;15(12):3527–3544. doi:10.1002/1878-0261.13079
38. Zhang Y, Tang J, Jiang C, et al. Metabolic reprogramming in cancer and senescence. *MedComm*. 2025;6(3):e70055. doi:10.1002/mco2.70055
39. Sideris M, Menon U, Manchanda R. Screening and prevention of ovarian cancer. *Med J Aust*. 2024;220(5):264–274. doi:10.5694/mja2.52227
40. Launonen IM, Vähärautio A, Färkkilä A. The emerging role of the single-cell and spatial tumor microenvironment in high-grade serous ovarian cancer. *Cold Spring Harb Perspect Med*. 2023;13(10):a041314. doi:10.1101/cshperspect.a041314
41. Tonti N, Golia D'Augè T, Cuccu I, et al. The role of tumor biomarkers in tailoring the approach to advanced ovarian cancer. *Int J Mol Sci*. 2024;25 (20):11239. doi:10.3390/ijms252011239
42. Nie X, Chen H, Xiong Y, Chen J, Liu T. Anisomycin has a potential toxicity of promoting cuproptosis in human ovarian cancer stem cells by attenuating YY1/lipoic acid pathway activation. *J Cancer*. 2022;13(14):3503–3514. doi:10.7150/jca.77445
43. Gan Y, Liu T, Feng W, et al. Drug repositioning of disulfiram induces endometrioid epithelial ovarian cancer cell death via the both apoptosis and cuproptosis pathways. *Oncology Research*. 2023;31(3):333–343. doi:10.32604/or.2023.028694
44. Shanbhag VC, Gudekar N, Jasmer K, et al. Copper metabolism as a unique vulnerability in cancer. *Biochim Et Biophysica Acta Mol Cell Res*. 2021;1868(2):118893. doi:10.1016/j.bbamcr.2020.118893
45. Zhang B, Xie L, Liu J, Liu A, He M. Construction and validation of a cuproptosis-related prognostic model for glioblastoma. *Front Immunol*. 2023;14:1082974. doi:10.3389/fimmu.2023.1082974
46. Kahlson MA, Dixon SJ. Copper-induced cell death. *Science*. 2022;375(6586):1231–1232. doi:10.1126/science.abo3959
47. Zhu W, Chen Z, Fu M, et al. Cuprotosis clusters predict prognosis and immunotherapy response in low-grade glioma. *Apoptosis*. 2024;29 (1–2):169–190. doi:10.1007/s10495-023-01880-y
48. Liu D, Yang F, Zhang T, Mao R. Leveraging a cuproptosis-based signature to predict the prognosis and drug sensitivity of cutaneous melanoma. *J Transl Med*. 2023;21(1):57. doi:10.1186/s12967-023-03891-4
49. Huang EM, Ma N, Ma T, et al. Cuproptosis-related long non-coding RNAs model that effectively predicts prognosis in hepatocellular carcinoma. *World J Gastrointest Oncol*. 2022;14(10):1981–2003. doi:10.4251/wjgo.v14.i10.1981
50. Ma S, Zhu J, Wang M, et al. A cuproptosis-related long non-coding RNA signature to predict the prognosis and immune microenvironment characterization for lung adenocarcinoma. *Transl Lung Cancer Res*. 2022;11(10):2079–2093. doi:10.21037/tlcr-22-660
51. Liu Y, Jiang J. A novel cuproptosis-related lncRNA signature predicts the prognosis and immunotherapy for hepatocellular carcinoma. *Cancer Biomark*. 2023;37(1):13–26. doi:10.3233/cbm-220259
52. Dawes AJ, Sacks GD, Needleman J, et al. Injury-specific variables improve risk adjustment and hospital quality assessment in severe traumatic brain injury. *The Journal of Trauma and Acute Care Surgery*. 2019;87(2):386–392. doi:10.1097/ta.0000000000002297

53. Huang Q, Lin Y, Chen C, et al. Immune-related LncRNAs affect the prognosis of osteosarcoma, which are related to the tumor immune microenvironment. *Front Cell Develop Biol*. 2021;9:731311. doi:10.3389/fcell.2021.731311
54. Qin M, Ma Y, Wang Z, Fang D, Wei J. Using immune-related lncRNAs to construct novel biomarkers and investigate the immune landscape of breast cancer. *Transl Cancer Res*. 2021;10(6):2991–3003. doi:10.21037/tcr-21-783
55. Ji J, Yin Y, Ju H, et al. Long non-coding RNA Lnc-Tim3 exacerbates CD8 T cell exhaustion via binding to Tim-3 and inducing nuclear translocation of Bat3 in HCC. *Cell Death Dis*. 2018;9(5):478. doi:10.1038/s41419-018-0528-7
56. Zheng Y, Yao M, Yang Y. Higher tumor mutation burden was a predictor for better outcome for NSCLC patients treated with PD-1 antibodies: a systematic review and meta-analysis. *SLAS Technology*. 2021;26(6):605–614. doi:10.1177/24726303211024557
57. Li Y, Ma Y, Wu Z, et al. Tumor mutational burden predicting the efficacy of immune checkpoint inhibitors in colorectal cancer: a systematic review and meta-analysis. *Front Immunol*. 2021;12:751407. doi:10.3389/fimmu.2021.751407
58. Deng H, Zhao Y, Cai X, et al. PD-L1 expression and tumor mutation burden as pathological response biomarkers of neoadjuvant immunotherapy for early-stage non-small cell lung cancer: a systematic review and meta-analysis. *Crit rev oncol/hematol*. 2022;170:103582. doi:10.1016/j.critrevonc.2022.103582
59. Bogani G, Moore KN, Ray-Coquard I, et al. Incorporating immune checkpoint inhibitors in epithelial ovarian cancer. *Gynecol Oncol*. 2025;193:30–40. doi:10.1016/j.ygyno.2024.12.011
60. Di DV, Caruso G, Perniola G, et al. Prognostic impact of microscopic residual disease after neoadjuvant chemotherapy in patients undergoing interval debulking surgery for advanced ovarian cancer. *Arch Gynecol Obstet*. 2025;311(2):429–436. doi:10.1007/s00404-024-07775-w
61. Zhou H, Gao Y, Li X, et al. Identifying and characterizing lincRNA genomic clusters reveals its cooperative functions in human cancer. *J Transl Med*. 2021;19(1):509. doi:10.1186/s12967-021-03179-5
62. Peng J, Zhu Y, Dong X, et al. Construction and analysis of lncRNA-associated ceRNA network identified potential prognostic biomarker in gastric cancer. *Transl Cancer Res*. 2019;8(4):1116–1128. doi:10.21037/tcr.2019.06.32
63. Wei C, Liang Q, Li X, et al. Bioinformatics profiling utilized a nine immune-related long noncoding RNA signature as a prognostic target for pancreatic cancer. *J Cell Biochem*. 2019;120(9):14916–14927. doi:10.1002/jcb.28754
64. Gao Q, Shi Y, Sun Y, et al. Identification and verification of aging-related lncRNAs for prognosis prediction and immune microenvironment in patients with head and neck squamous carcinoma. *Oncology Research*. 2023;31(1):35–61. doi:10.32604/or.2022.028193
65. Rodríguez-Bautista R, Caro-Sánchez CH, Cabrera-Galeana P, et al. Immune milieu and genomic alterations set the triple-negative breast cancer immunomodulatory subtype tumor behavior. *Cancers*. 2021;13(24):6256. doi:10.3390/cancers13246256
66. Hu W, Wang Y, Fang Z, He W, Li S. Integrated characterization of lncRNA-immune interactions in prostate cancer. *Front Cell Develop Biol*. 2021;9:641891. doi:10.3389/fcell.2021.641891